Supramolecular Chemistry
Vol. 22, Nos. 11–12, November–December 2010, 870–890

Taylor & Francis
Taylor & Francis Group

Anion binding, aryl-extended cyclotriguaiacylenes and an aryl-bridged cryptophane that provides snapshots of a molecular gating mechanism†

K. Travis Holman[a]*, Stephen D. Drake[a], Jonathan W. Steed[b], G. William Orr[c] and Jerry L. Atwood[c]

[a]*Department of Chemistry, Georgetown University, 37th and O Streets NW, Washington, DC 20057, USA;* [b]*Department of Chemistry, Durham University, South Road, Durham DH1 3LE, UK;* [c]*Department of Chemistry, University of Missouri, 601 S. College Ave., Columbia, MO 65211, USA*

(*Received 29 June 2010; final version received 2 August 2010*)

Cyclotriguaiacylene, (±)-**CTG**, reacted with a series of $[(\eta^5\text{-}C_5H_5)Fe^{II}(\eta^6\text{-chloroarenes})]^+$ to yield a family of aryl-extended, $[(\eta^5\text{-}C_5H_5)Fe^{II}]^+$-functionalised cavitands (±)-$\mathbf{2}^{3+}$. Crystal structures of $[BF_4]^-$ or mixed $[BF_4]^-/[PF_6]^-$ salts of these cavitands shed light on their conformational dynamics and anion binding properties. These hosts adopt conformations that project the $[(\eta^5\text{-}C_5H_5)Fe^{II}(\eta^6\text{-arene})]^+$ substituents 'up' from the rim of the cavitand, creating deep cavities that are occupied by a $[BF_4]^-$ anion. Hosts (±)-$\mathbf{2a}$–$\mathbf{f}^{3+}$ appear to show some selectivity for the formation of penetrated ion pairs with $[BF_4]^-$ in preference to $[PF_6]^-$. The compounds were photochemically demetalated, giving aryl-extended CTGs (±)-**3a**–**d**,**f**. The crystal structure of (±)-**3a** reveals that the molecule forms a centrosymmetric, self-included dimer in the solid state. Cryptophanes *syn*-**5** and (±)-*anti*-**4** were synthesised by the photochemically induced demetalation of the putative metalated cryptophanes *syn*-**4**$[PF_6]_3$ and (±)-*anti*-**4**$[PF_6]_3$, obtained by the 'capping' of the cavitand (±)-$\mathbf{2d}^{3+}$ by (±)-**CTG**. Single crystal structures of five different solvates of (±)-*anti*-**5** reveal host–guest encapsulated complexes that are interpreted as revealing 'snapshots' of the molecular gating process. The first crystallographically characterised example of an empty cryptophane, namely (±)-*anti*-**5**, reveals that this host can also readily adopt a conformation that fills the bulk of its own cavity.

Keywords: cyclotriveratrylene; cryptophane; encapsulation; gating; penetrated ion pair

Introduction

[1.1.1]-Orthocyclophane-based macrocycles, i.e. cyclotribenzylenes (CTBs, a subset of which are shown in Scheme 1), have been known for at least 150 years (*1*). Present-day interest is commonly associated with the more or less rigid (*2*, *3*), bowl-shaped – i.e. cavitand (*4*) – structure of the CTB scaffold in the context of supramolecular chemistry, where these concave hosts can be exploited for the complexation of various guests. Indeed, CTBs are among the most studied macrocycles in the field (*5*). The cavities of the CTBs have been extensively employed for the complexation of fullerenes (*6*), cations (*7*) and even anions (*8–11*). CTB derivatives have also been used as liquid crystal mesogens (*12*), to construct monolayers on surfaces (*13*) or at the air–solution interface (*14*), in dendrimers (*15*), organic/metallogels (*16*) and other soft materials (*17*). Moreover, like other cavitands, the inability of many CTBs to close-pack in the solid state has led to their extensive study in solid-state organic chemistry, forming, for example, crystalline inclusion compounds (*18–20*) or polymers of intrinsic microporosity (*21*). Also of particular interest are the cryptophanes (Scheme 1) (*22*, *23*) – Collet's family of container molecule hosts constructed by the joining of two CTB cavitands – and related higher order container-like structures derived from the dynamic covalent chemistry (*24*) (including metal–ligand self-assembly (*25*, *26*)) of various CTB derivatives. These and other so-called container molecules (*4*, *27*) have captured much attention in recent years related to their ability to selectively encapsulate and/or organise guests and the relatively high kinetic stabilities of the corresponding host–guest complexes, allowing complexes of low thermodynamic stability to be sufficiently long-lived for spectroscopic observation. The lifetimes of container molecule complexes are attributable to the nearly closed-surface structures of the hosts: the host imposes a physical barrier to guest exchange, effectively gating access to the internal cavity. For very recent reviews concerning advances in cryptophane chemistry and in the supramolecular chemistry of CTBs in general, the reader is referred to those of Brotin and Dutasta (*23*), and Hardie (*5*), respectively.

Among the more synthetically useful CTBs that serve as scaffolds for chemical functionalisation are the C_{3v} symmetric cyclotriveratrylene (CTV, Scheme 1, $R_1 = R_2 = OCH_3$) and cyclotricatechylene (Scheme 1,

*Corresponding author. Email: kth7@georgetown.edu
†This paper is contributed in memory of Prof. Dmitry M. Rudkevich, who positively influenced our thinking in so many ways.

ISSN 1061-0278 print/ISSN 1029-0478 online

DOI: 10.1080/10610278.2010.514615
http://www.informaworld.com

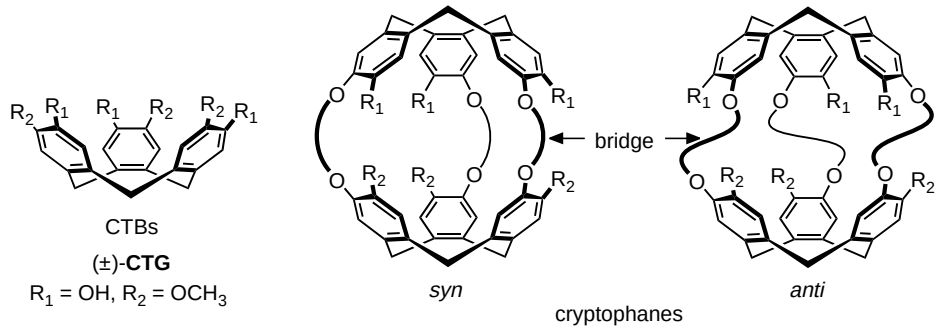

Scheme 1. The general structures of cyclotribenzylenes (CTBs) and cryptophanes.

$R_1 = R_2 = OCH_3$), and the chiral, C_3 symmetric cyclotrianisidine ((±)-CTA, Scheme 1, $R_1 = NH_2$, $R_2 = OCH_3$) and cyclotriguaiacylene ((±)-**CTG**, Scheme 1, $R_1 = OH$, $R_2 = OCH_3$) cavitands (*28*). The latter, (±)-**CTG**, is of particular importance as it constitutes the structural subunit of most cryptophanes, its chirality giving rise to *syn* and *anti* cryptophane diastereomers. Moreover, (±)-**CTG** constitutes the precursor to a variety of chiral, C_3 symmetric CTB derivatives via functionalisation of the phenolic residues. Our work in the area of anion complexation (*29*) by organometallic sandwich compounds of cavitands (*10*), e.g. $[(\eta^6\text{-arene})Ru^{II}]^{2+}$ or $[(\eta^5\text{-}C_5Me_5)Ir/Rh^{III}]^{2+}$-functionalised CTVs (*8*), or calix[*n*]-arenes (*30*), and, more recently, $[(\eta^5\text{-}C_5Me_5)Ru^{II}]^{+}$-functionalised cryptophanes (*11*) (Scheme 2), led us, some time ago, to pursue deep cavity, upper rim $[(\eta^5\text{-}C_5H_5)Fe(\eta^6\text{-arene})]^{+}$-functionalised CTBs via the nucleophilic aromatic substitution (S_NAr) of $[(\eta^5\text{-}C_5H_5)Fe(\eta^6\text{-chloroarenes})]^{+}$ by (±)-**CTG** (e.g. (±)-$\mathbf{2}^{3+}$ in Scheme 2) (*9*). Notably, based upon the premise that limited conformational flexibility would likely impart anion selectivity, an important part of the design strategy leading to cavitands (±)-$\mathbf{2}^{3+}$ was the incorporation of aryl ether moieties, as opposed to, say, benzylic ether moieties at the upper rim of the CTB cavitand. At the time, (±)-$\mathbf{2}^{3+}$ were the first examples of aryl-functionalised **CTG**s and a number of such compounds, also derived from the S_NAr substitution of electron-deficient haloarenes by (±)-**CTG**, have since been reported by Pochini and co-workers (*31*). Concerning host design, it also occurred to us that unique, potentially anion-encapsulating cryptophanes such as (±)-*anti*-$\mathbf{4}^{3+}$ should be available from compounds (±)-$\mathbf{2}^{3+}$ (Scheme 2, X = Cl) by the capping of these cavitands with another (±)-**CTG** moiety. The anion hosts in Scheme 2 are comparable to the family of anion binding/sensing organometallic cavitands developed by Beer and co-workers (*32*), except that anion complexation is not assisted by the presence of traditional hydrogen bond donor functionalities. Moreover, being constructed almost entirely of arenes, many of the hosts shown in Scheme 2 are of contemporary relevance in the context of recent/renewed interest in the interactions between anions

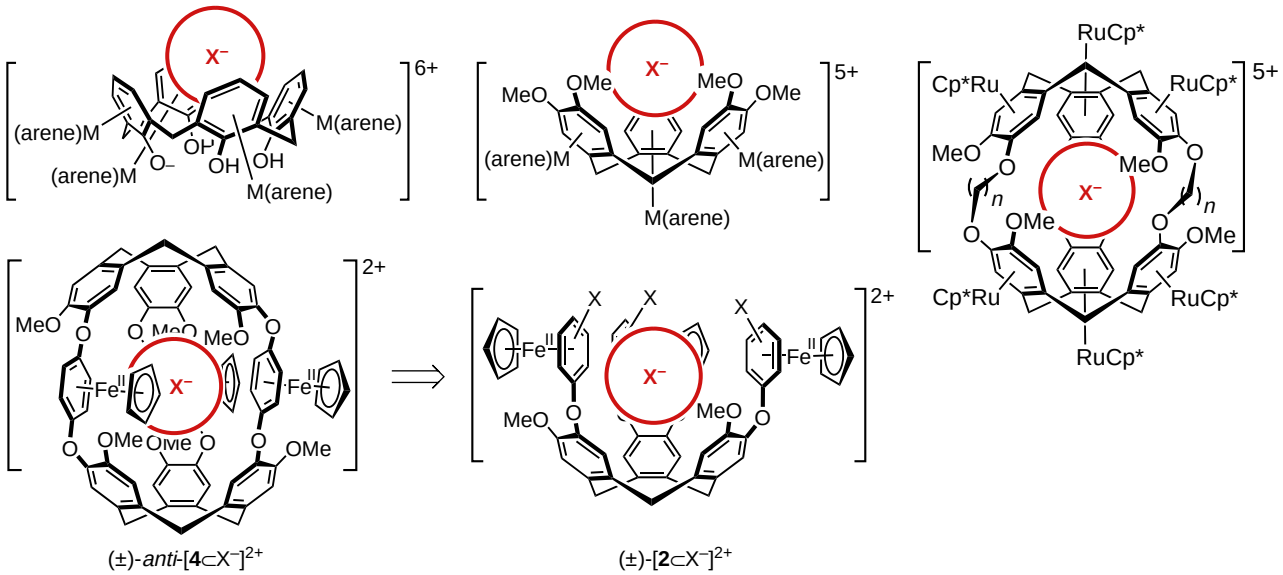

Scheme 2. Anion-binding, organometallic cavitands and cryptophanes.

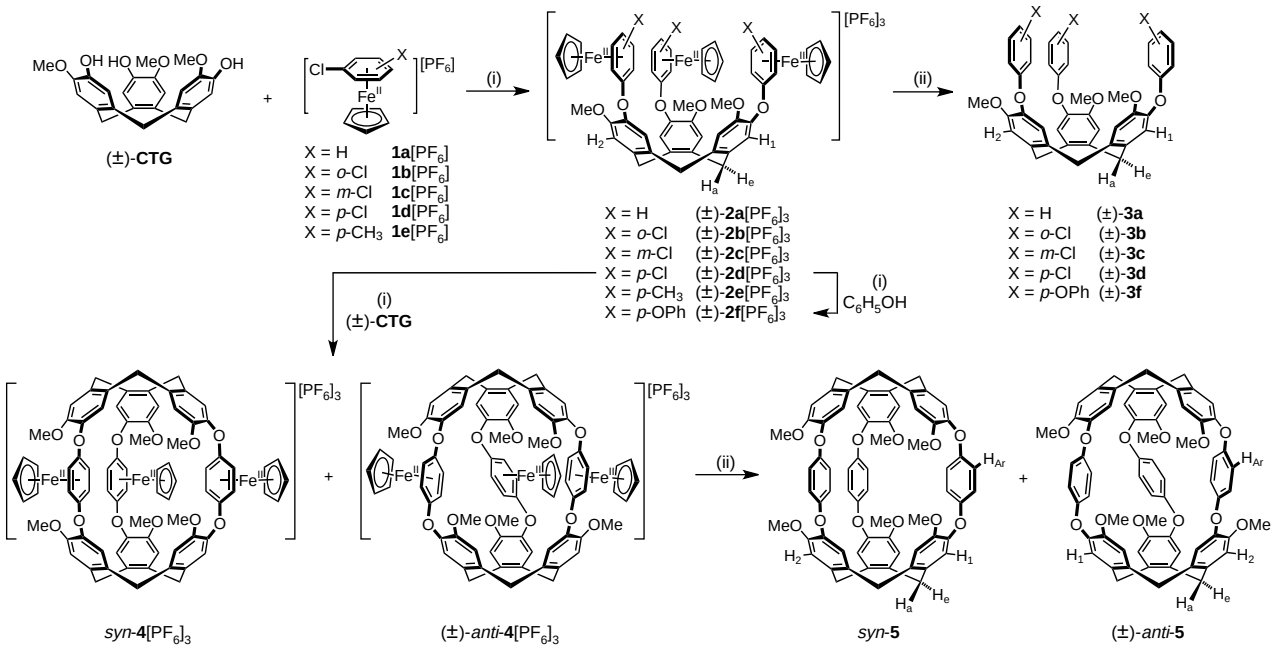

Figure 1. Synthesis of aryl-extended CTGs and aryl-bridged cryptophanes. (i) K_2CO_3, DMF, room temperature; (ii) $h\nu$, CH_3CN.

and arenes, as they are early examples of hosts that bind anions via a charge-assisted form of the so-called anion–π interaction (*33*).

Herein, we describe a number of new aryl-extended CTGs derived from the organometallic compounds (±)-**2**$^{3+}$ by the photochemically induced removal of the $[(\eta^5\text{-}C_5H_5)Fe^{II}]^+$ moieties (Figure 1). We also report indirect evidence for the achievement of $[(\eta^5\text{-}C_5H_5)Fe(\eta^6\text{-arene})]^+$-bridged cryptophanes, e.g. (±)-*anti*-**4**$^{3+}$, by isolating their photochemically demetalated cryptophane products. New single crystal structures of salts of [(±)-**2**]$^{3+}$ provide insights into their anion complexation properties and single crystal structures of the corresponding cryptophane solvates reveal host conformations that can reasonably be interpreted as representing 'snapshots' of the molecular gating mechanism in this important family of supramolecular container compounds. We note that other deep cavity, C_3 symmetric cavitands and containers have been investigated in the context of their molecular gating mechanisms (*34*). Moreover, oligo(*p*-phenylene oxides)s are of general interest in supramolecular host–guest (*35*) and solid-state organic chemistry (*36*).

Results and discussion

Synthesis and characterisation

The general synthetic scheme adopted for the work presented herein is given in Figure 1. For a review on the use of π-organoiron complexes in arene chemistry, the reader is referred to that by Astruc (*37*). Deep cavity, upper rim $[(\eta^5\text{-}C_5H_5)Fe(\eta^6\text{-arene})]^+$-functionalised CTGs (±)-**2a**–**e**[PF_6] were synthesised by an adaptation of the procedure reported by Abd-El-Aziz and co-workers for the synthesis of oligomeric (*38*) and cyclic (*39*) aryl ethers possessing pendant cyclopentadienyliron moieties. Racemic cyclotriguaiacylene, (±)-**CTG**, was reacted at room temperature with the appropriate $[(\eta^5\text{-}C_5H_5)Fe(\eta^6\text{-chloroarene})][PF_6]$ salt, **1**[PF_6], in dry dimethyl formamide (DMF) in the presence of potassium carbonate. Notably, the reactive chloro substituents at the upper rim of (±)-**2d**$^{3+}$ provide a site for further cavity extension. Thus, extended (±)-**2f**$[PF_6]_3$ was obtained by reaction of the *para*-chloro-functionalised (±)-**2d**$[PF_6]_3$ with phenol under similar conditions.

Each new cavitand (±)-**2a**–**f**$[PF_6]_3$ was characterised by ^1H and ^{19}F NMR spectroscopy, as well as by single crystal X-ray diffraction whenever possible. The results of combustion elemental analyses were commonly unsatisfactory (see Experimental section). The ^1H NMR spectra of these compounds deserve comment as they are often complicated by anion binding behaviour, which is highly solvent dependent. The corresponding spectral features provide a handle for the monitoring of anion binding behaviour, as discussed in the following section. It is important to recognise that (±)-**2b**,**c**$[PF_6]_3$ are likely obtained as a mixture of all possible stereoisomers that can arise from the presence of helical chirality at the (±)-**CTG** moiety and the introduction of planar chirality at each of the three metalated, unsymmetrically 1,2-substituted (**2b**$[PF_6]_3$) or 1,3-substituted (**2c**$[PF_6]_3$) $[(\eta^5\text{-}C_5H_5)Fe^{II}(\eta^6\text{-arene})]^+$ moieties. Thus, while denoted simply as (±)-**2b**,**c**$[PF_6]_3$ in Figure 1, (±)-**2b**$[PF_6]_3$ and (±)-**2c**$[PF_6]_3$ are in fact a mixture of four diastereomers and

their enantiomers. For example, if one uses *P*/*M* descriptors to ascribe the stereochemistry of the (±)-**CTG** moieties and *R*/*S* descriptors to ascribe the stereochemistry of each of the three $[(\eta^5\text{-}C_5H_5)Fe^{II}(\eta^6\text{-arene})]^+$ moieties, then (±)-**2b**$[PF_6]_3$ is truly a mixture (likely statistical) of the *RRRM*-**2b**$[PF_6]_3$, *RRSM*-**2b**$[PF_6]_3$, *RSSM*-**2b**$[PF_6]_3$ and *SSSM*-**2b**$[PF_6]_3$ diastereomers and their enantiomers – a total of eight unique compounds. No attempts were made to separate or quantify the relative amounts of these diastereomers. Consequently, and as expected, (±)-**2b**,**c**$[PF_6]_3$ give rise to complicated and/or broad ^{1}H NMR spectra, as described in the Experimental section. Their ^{1}H NMR spectra are therefore either broadened substantially or extremely complicated as most peaks appear as multiplets.

An advantage of employing $[(\eta^5\text{-}C_5H_5)\text{-}Fe^{II}(\eta^6\text{-arene})]^+$ moieties in the synthesis of aryl ethers is that the $[(\eta^5\text{-}C_5H_5)Fe^{II}]^+$ substituents can, in general, be readily removed from the arene ring (*38*, *40*). Visible light photolysis is the method of choice. Accordingly, photolysis of the $[(\eta^5\text{-}C_5H_5)Fe(\eta^6\text{-arene})]^+$-functionalised cavitands (±)-**2a**–**d**,**f**$[PF_6]_3$ with direct sunlight in degassed acetonitrile yields the demetalated products (±)-**3a**–**d**,**f** in good to near-quantitative yields (Figure 1). Importantly, the near quantitative yields of (±)-**3b**,**c** (97% each) serve to further establish the structures and purity of the diastereomeric mixtures of (±)-**2b**,**c**$[PF_6]_3$, which give very complicated ^{1}H NMR spectra due to their stereochemistry (*vide supra*). Removal of the $[(\eta^5\text{-}C_5H_5)Fe^{II}]^+$ moieties from (±)-**2b**,**c**$[PF_6]_3$ reduces the number of stereocentres from four to only one, the (±)-**CTG** moiety, such that (±)-**3b**,**c** are easily characterised as a racemic mixture. Compounds (±)-**3a**–**d**,**f** gave expected ^{1}H and ^{13}C NMR spectra and satisfactory analysis for C and H elemental composition. For each compound, the upper rim arene substituents apparently rotate rapidly on the ^{1}H NMR timescale and arene ring rotation could not be 'frozen out', even at low temperatures (−70°C) in $CDCl_3$. This is perhaps not surprising, given that typical barriers to rotation about the O—C bonds of diphenyl ethers are very low – of the order of about ~20 kJ mol^{-1} ($\Delta H^{\ddagger} \approx 2$–10 kJ mol^{-1}) – even at 150 K in a solid matrix (*41*). It was initially hoped that, analogous to other CTBs, the new deep cavity-functionalised CTGs (±)-**3a**–**d**,**f** might be exploited for the selective binding of fullerenes (*6*). All attempts at such applications, however, proved unsuccessful, likely in consequence to the cavity-blocking effect of the conformationally mobile upper rim aryl rings.

In order to investigate the conformational preferences of cavitands (±)-**3a**–**d**,**f** – at least in the solid state – several attempts were made to grow single crystals of these compounds, but, with the exception of (±)-**3a**, sufficiently large single crystals were not obtained. The X-ray crystal structure of (±)-**3a** was determined and a thermal ellipsoid plot of the molecule is depicted in Figure 2.

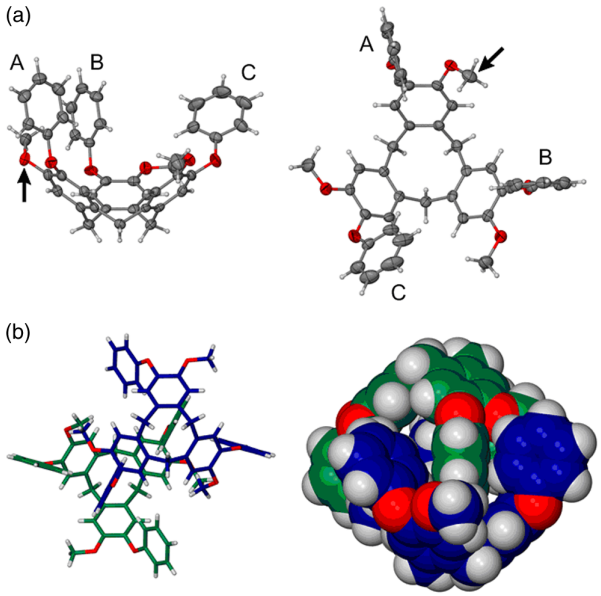

Figure 2. The X-ray crystal structure of (±)-**3a** showing (a) top and side views of the molecular structure (50% probability thermal ellipsoids) and (b) the self-included dimer.

Summary data for all X-ray structure determinations are given in Table 1. The upper rim aryl substituents are all directed 'upward' from the rim of the **CTG** bowl. For two of these arene rings, A and B, the mean plane of the arene ring is nearly orthogonal to the mean plane of the cavitand upper rim, as defined by the oxygen atoms of the diphenyl ether moieties. The corresponding interplanar angles, defined hereafter as ϕ, measure 90° and 89° for rings A and B, respectively. The third ring, C, is turned significantly out of plane relative to the cavitand oxygen atoms (ϕ = 57°), but its carbon atoms nonetheless reside entirely above the upper rim of the cavitand. The arene–arene dihedral angles of the three diphenyl ether moieties, involving rings A, B and C, respectively, measure 77°, 73° and 72°. Perhaps surprisingly, and unlike many other CTB-based cavitands, (±)-**3a** does not form an inclusion compound with the solvent employed for crystallisation, in this case toluene. Instead, an interesting form of self-inclusion is observed, in which one of the upper rim arene rings of one molecule (ring B) is directed into the molecular cavity of its enantiomer. Two molecules of (±)-**3a** thus form a sort of centrosymmetric dimer in the solid state, with each occupying the molecular cavity of the other. The cavity-included arene rings are involved in numerous edge-to-face interactions with the arene rings that form the walls of the cavity. Lastly, and as is previously observed in some CTV inclusion compounds (*42*), one of the methoxy substituents (indicated by an arrow in Figure 2) is distorted from the plane of the arene ring, by 58° in this instance.

Table 1. Summary data for X-ray single crystal structure determinations.

Compound	(±)-**2a**$[BF_4][PF_6]_2\cdot(THF)\cdot(CH_3COCH_3)$[a]	(±)-**2d**$[BF_4]_3\cdot(CH_3COCH_3)$	(±)-**2e**$[BF_4]_3\cdot(CH_3COCH_3)$
Formula	$C_{64}H_{65}O_8BF_{16}P_2Fe_3$	$C_{60}H_{54}O_7B_3F_{12}Cl_3Fe_3$	$C_{63}H_{63}O_7B_3F_{12}Fe_3$
Formula weight (g mol^{-1})	1506.49	1421.40	1360.14
Crystal system	Monoclinic	Monoclinic	Monoclinic
Space group	$P2_1/n$	$P2_1/n$	$P2_1/n$
Temperature (K)	173	173	173
a (Å)	9.5929(5)	9.3918(6)	9.5292(2)
b (Å)	21.562(1)	20.815(1)	20.541(1)
c (Å)	30.579(2)	31.311(2)	31.532(2)
α (°)	90	90	90
β (°)	90.769(1)	90.521(1)	90.670(1)
γ (°)	90	90	90
V (Å^3)	6324.4(6)	6120.9(7)	6171.5(5)
Z	4	4	4
ρ_{calc} (g cm^{-3})	1.58	1.54	1.46
μ[Mo Kα] (cm^{-1})	8.30	9.19	7.84
Reflns coll/unique/obs	20,157/8729/5547	24,732/8431/6093	19,815/8489/5646
Parameters/restraints	921/474	829/456	839/6
$2\theta_{max}$ (°)	46	46	46
R (int)	0.0432	0.0425	0.0554
R_1, wR_2 [$I > 2\sigma(I)$]	0.091, 0.247	0.073, 0.203	0.080, 0.187
R_1, wR_2 (all)	0.126, 0.275	0.102, 0.225	0.125, 0.211
Residual (e$^-$ Å^{-3})	0.82	1.44 (near BF_4^-)	1.12 (near BF_4^-)

Compound	(±)-**2f**$[BF_4]_2[PF_6]$	**2g**$[PF_6]$	**2h**$[PF_6]\cdot$DMF
Formula	$C_{75}H_{63}O_9B_2F_{14}PFe_3$	$C_{19}H_{19}O_3F_6PFe$	$C_{30}H_{34}NO_7F_6PFe$
Formula weight (g mol^{-1})	1594.43	496.17	721.41
Crystal system	Monoclinic	Triclinic	Monoclinic
Space group	$P2_1/c$	P-1	$P2_1/c$
Temperature (K)	173	173	173
a (Å)	9.2715(5)	8.7171(7)	8.5426(5)
b (Å)	20.649(1)	11.0856(9)	18.396(1)
c (Å)	36.446(2)	11.5144(9)	19.572(1)
α (°)	90	107.773(1)	90
β (°)	93.424(1)	93.041(1)	98.438(1)
γ (°)	90	109.163(1)	90
V (Å^3)	6064.9(6)	986.2(1)	3042.4(3)
Z	4	2	4
ρ_{calc} (g cm^{-3})	1.52	1.67	1.57
μ[Mo Kα] (cm^{-1})	7.36	9.20	6.22
Reflns coll/unique/obs	22,194/9551/5803	41,20/3370/2901	15,169/5310/3787
Parameters/restraints	932/316	320/12	467/0
$2\theta_{max}$ (°)	46	50	50
R (int)	0.0539	0.0115	0.0386
R_1, wR_2 [$I > 2\sigma(I)$]	0.091, 0.228	0.054, 0.154	0.077, 0.223
R_1, wR_2 (all)	0.147, 0.260	0.060, 0.159	0.099, 0.239
Residual (e$^-$ Å^{-3})	0.53	0.56	0.61

Compound	(±)-**3a**	(±)-*anti*-**5**$\cdot(CHCl_3)_4$	(±)-*anti*-**5**$\cdot(C_6H_5NO_2)_5$
Formula	$C_{42}H_{36}O_6$	$C_{70}H_{58}O_{12}Cl_{12}$	$C_{96}H_{79}O_{22}N_5$
Formula weight (g mol^{-1})	636.75	1516.66	827.35
Crystal system	Monoclinic	Triclinic	Monoclinic
Space group	$P2_1/n$	P-1	$C2/c$
Temperature (K)	173	173	173
a (Å)	13.142(3)	12.3672(8)	31.180(2)
b (Å)	12.727(3)	13.8257(9)	13.930(1)
c (Å)	19.553(5)	20.075(1)	22.680(3)
α (°)	90	83.807(1)	90
β (°)	94.280(5)	87.628(1)	126.116(1)
γ (°)	90	84.960(1)	90
V (Å^3)	3261(1)	3397.6(4)	7961.5(2)
Z	4	2	4

Table 1 – *continued.*

Compound	(±)-**3a**	(±)-*anti*-**5**·$(CHCl_3)_4$	(±)-*anti*-**5**·$(C_6H_5NO_2)_5$
ρ_{calc} (g cm^{-3})	1.30	1.48	1.38
μ[Mo Kα] (cm^{-1})	0.86	5.51	0.97
Reflns coll/unique/obs	17,127/5732/2720	10,997/8896/6040	24,810/7014/5479
Parameters/restraints	436/0	900/102	577/30
$2\theta_{max}$ (°)	50	50	56
R (int)	0.0918	0.0319	0.0392
R_1, wR_2 [$I > 2\sigma(I)$]	0.046, 0.090	0.099, 0.253	0.044, 0.107
R_1, wR_2 (all)	0.107, 0.105	0.137, 0.286	0.062, 0.118
Residual (e$^-$ Å^{-3})	0.19	1.33 (near Cl)	0.26
Compound	(±)-*anti*-**5**·$(C_6H_5N)_{5^{2/3}}$[a]	(±)-*anti*-**5**·$(C_6H_5Cl)_{2.5}$	(±)-*anti*-**5**·$(CHCl_3)_2$·$(TCE)_2$
Formula	$C_{96^{1/3}}H_{82^{1/3}}O_{12}N_{5^{2/3}}$	$C_{81}H_{66.5}O_{12}Cl_{2.5}$	$C_{36}H_{30}O_6Cl_7$
Formula weight (g mol^{-1})	1513.41	1334.55	806.80
Crystal system	Hexagonal	Triclinic	Monoclinic
Space group	*R*-3*c*	*P*-1	*C*2/*c*
Temperature (K)	173	173	173
a (Å)	16.4495(6)	12.4658(7)	17.940(1)
b (Å)	16.4495(6)	13.1646(8)	18.774(1)
c (Å)	49.844(3)	22.426(1)	22.528(1)
α (°)	90	76.684(1)	90
β (°)	90	79.864(1)	102.580(1)
γ (°)	120	63.664(1)	90
V (Å^3)	11680.2(9)	3198.1(3)	7405.5(7)
Z	6	2	8
ρ_{calc} (g cm^{-3})	1.29	1.39	1.45
μ[Mo Kα] (cm^{-1})	0.85	1.91	5.81
Reflns coll/unique/obs	12,208/1810/1595	10,644/8546/6081	14,649/6480/4512
Parameters/restraints	160/0	895/0	442/0
$2\theta_{max}$ (°)	46	50	50
R (int)	0.0283	0.0217	0.0368
R_1, wR_2 [$I > 2\sigma(I)$]	0.058, 0.151	0.104, 0.295	0.054, 0.133
R_1, wR_2 (all)	0.064, 0.157	0.134, 0.322	0.978, 0.145
Residual (e$^-$ Å^{-3})	0.30	0.75	0.66

[a] This structure was treated with SQUEEZE to model highly disordered solvents.

That certain substituted benzyl alcohols can be directly trimerised to form CTBs led us to synthesise **2g**[PF_6] and **2h**[PF_6] by the reaction of excess vanillyl alcohol with either **1a**[PF_6] or **1d**[PF_6], respectively (Figure 3). **2g**[PF_6] and **2h**[PF_6] were characterised by ^{1}H, ^{13}C and ^{19}F NMR spectroscopy and by single crystal structure determinations. The cations from these structures are depicted in Figure 3. In practice, the cyclotrimerisation of substituted benzyl alcohols, or the reaction of arenes with a formaldehyde equivalent, to yield CTBs is governed by the identity of the arene ring substituents. In general, electron-donating substituents at the 3,4-positions are necessary for cyclotrimerisations of benzyl alcohols to proceed in reasonable yields (*28*). Typically, the role of the substituent at the 3-position (commonly $-OCH_3$) is to activate the *para*-position (*ortho* to the benzylic group) for electrophilic attack and the role of the substituent at the 4-position (e.g. OCH_2COOH, $OCH_2CH{=}CH_2$, Br, SCH_3, NHCOMe) is largely to inhibit side reactions at this site (*43*). Substituted vanillyl alcohols (4-substituted-3-methoxy-benzyl alcohols) are good candidates for direct, acid-catalysed cyclotrimerisation, and it was conceivable that **2g**[PF_6] – a 3-methoxy-4-[(η^5-C_5H_5)Fe^{II}(η^6-C_6H_5O-)]$^+$-substituted benzyl alcohol – could be directly cyclotrimerised to (±)-**2a**[PF_6]$_3$. Similarly, it was conceivable that **2h**[PF_6] might provide a direct route to metalated cryptophanes *syn*-**4**[PF_6]$_3$ and/or (±)-*anti*-**4**[PF_6]$_3$ in an approach analogous to Collet's so-called 'two-step' method of cryptophane synthesis (*44*). Alternatively, the photodemetalated products of **2g**[PF_6] or **2h**[PF_6] – i.e. the corresponding 4-aryloxy-3-methoxy-substituted benzyl alcohols – were also plausible precursors for direct cyclotrimerisation to (±)-**3a** or cryptophanes *syn*-**5** and/or (±)-*anti*-**5**, respectively. Unfortunately, all attempts at the acid-catalysed (e.g. 65% $HClO_4$ or formic acid) cyclisation of **2g**[PF_6] or **2h**[PF_6] failed and only starting materials were recovered. The apparent lack of a reaction might be attributed to a difficulty in forming the required benzyl cation intermediate in consequence to the fact that a positive charge is already present on the molecule in the form of the [(η^5-C_5H_5)Fe^{II}(η^6-arene-)]$^+$ moiety. Unfortunately, also, attempts to cleanly displace the [(η^5-C_5H_5)Fe^{II}]$^+$ moieties

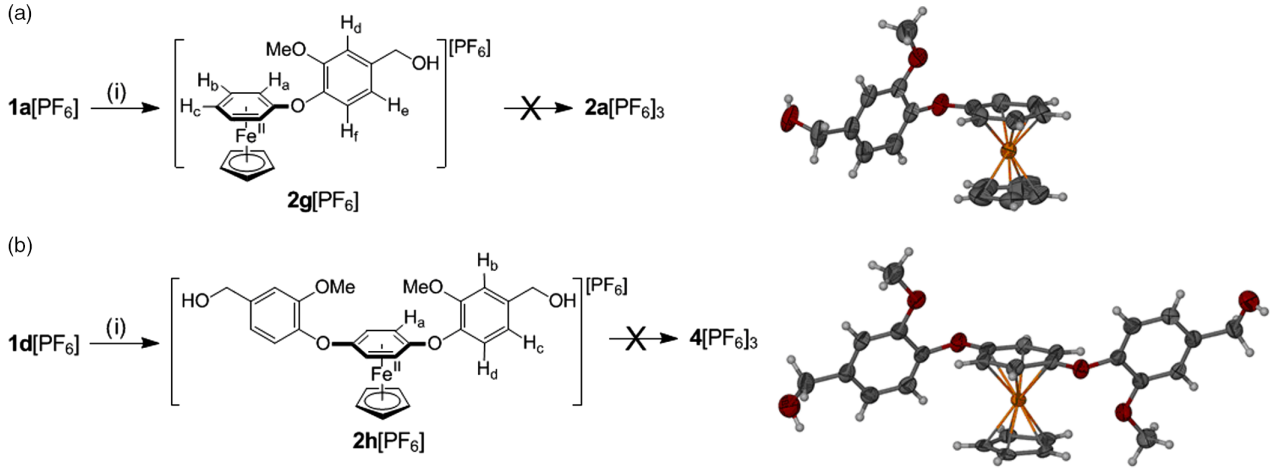

Figure 3. Synthesis of potential CTB and cryptophane precursors **2g**[PF_6] and **2h**[PF_6]: (i) K_2CO_3, DMF, excess vanillyl alcohol. Thermal ellipsoid plots of the cations from the X-ray crystal structures of (a) **2g**[PF_6] and (b) **2h**[PF_6]·DMF. The $[(\eta^5\text{-}C_5H_5)Fe^{II}]^+$ moiety of $\mathbf{2h}^+$ is disordered about the two faces of the coordinated arene. Only the major occupancy portion (80%) is shown.

from **2g**[PF_6] or **2h**[PF_6] by photochemical means (sunlight, CH_3CN) were equally unsuccessful.

Of the now hundreds of known cryptophanes, most are synthesised by one of two methods (*22*, *23*): (i) the so-called 'template' method whereby three appropriately substituted benzyl alcohol moieties are first appended to the upper rim of a pre-formed CTB cavitand and are then cyclotrimerised, the pre-formed CTB serving as a template for cyclisation of the second; or (ii) the 'two-step' method whereby two appropriately substituted benzyl alcohol moieties (usually vanillyl alcohols) are first covalently linked via some bridge and are then simultaneously cyclotrimerised. A third, less conventional approach involves the 'capping' of a pre-formed CTB cavitand with another pre-formed CTB. Cram et al. (*45*) first used the capping approach successfully in the copper-catalysed coupling of two terminal acetylene-functionalised CTBs to give the corresponding cryptophanes. More recently, the smallest cryptophane, so-called cryptophane-1.1.1, was synthesised by a capping method (*46*). Xu and Warmuth (*24*) have also recently exploited dynamic covalent chemistry to adjoin two pre-formed CTBs, resulting in amine-bridged cryptophanes. Shinkai et al. (*25*) have used a related capping approach, taking advantage of the transition metal coordination chemistry of CTB-based ligands.

Our inability to cyclise **2g**[PF_6] or **2h**[PF_6] necessitated a capping approach for the synthesis of the corresponding cryptophanes *syn*-**4**[PF_6]$_3$, (±)-*anti*-**4**[PF_6]$_3$ and ultimately *syn*-**5** and (±)-*anti*-**5**. The 1,4-arylether-bridged cryptophanes were synthesised by the capping of the 4-chloro terminal (±)-**3d**[PF_6]$_3$ with an additional equivalent of (±)-**CTG** (Figure 1). The reaction was accomplished at low concentrations (3.0 mM) in basic DMF, yielding after work-up, a yellow solid that, by ^{1}H NMR spectroscopy, appeared to consist mostly of poly/oligomeric material. Somewhat surprisingly, the ^{19}F NMR spectrum of this material showed only one doublet corresponding to the $[PF_6]^-$ counterions and thus, contrary to our expectations, the putative *syn*-**4**[PF_6]$_3$ and/or (±)-*anti*-**4**[PF_6]$_3$ cryptophanes seemingly do not incarcerate $[PF_6]^-$ anions upon shell closure. Presumed, nonetheless, to contain the desired *syn*-**4**[PF_6]$_3$ and (±)-*anti*-**4**[PF_6]$_3$, and lacking a suitable means for separation of these cryptophanes from the poly/oligomeric material, the product mixture was subjected to sunlight photolysis in degassed CH_3CN in order to remove the $[(\eta^5\text{-}C_5H_5)Fe^{II}]^+$ moieties. Work-up by column chromatography yielded mixtures of the two cryptophane diastereomers *syn*-**5** and (±)-*anti*-**5**, which were further separated by fractional crystallisation, giving unoptimised yields of 3 and 7%, respectively – yields that are somewhat typical of other cryptophane syntheses. By inference, the successful isolation of *syn*-**5** and (±)-*anti*-**5** unequivocally establishes the existence of *syn*-**4**[PF_6]$_3$ and (±)-*anti*-**4**[PF_6]$_3$, though we have not as yet been successful in isolating these cryptophanes.

Syn-**5** and (±)-*anti*-**5** were characterised by ^{1}H and ^{13}C NMR spectroscopy, elemental analysis ((±)-*anti*-**5** only) and single crystal X-ray diffraction (*vide infra*). Though readily discernable in most solvents, the ^{1}H NMR spectra of *syn*-**5** and (±)-*anti*-**5** (Figure 4) are nearly identical, reflecting the identical symmetry-unique portions (i.e. fundamental regions) of the two molecules and the equivalent order (6) of their respective C_{3h} and D_3 point group symmetries. Notably, protons of the *meso* form, *syn*-**5**, resonate downfield from (±)-*anti*-**5** in most solvents. Also notable is the observation that the protons of the 1,4-dioxylaryl bridge of both diastereomers appear as a singlet in the ^{1}H NMR spectrum, indicating, analogous to the aryl-functionalised **CTG**s (±)-**3**, fast rotation of the arene bridges on the ^{1}H NMR timescale, even at temperatures as low as −65°C. Unambiguous assignment of the diastereomers was easily accomplished by crystal

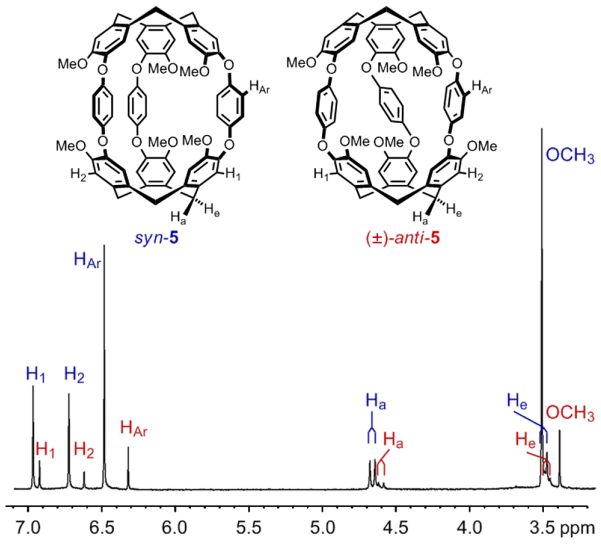

Figure 4. ^{1}H NMR spectrum (400 MHz, $CDCl_3$) of an approximate 5:1 mixture of *syn*-**5** and (±)-*anti*-**5**.

structure determinations. Vapour diffusion of *n*-hexane into a solution of (±)-*anti*-**5** in $CHCl_3$ results in well-formed single crystals of composition (±)-*anti*-**5**·4$CHCl_3$. X-ray analysis of (±)-*anti*-**5**·4$CHCl_3$ and several other solvates (Table 1, *vide infra*) confirmed the *anti* stereochemistry of the host. Moreover, a low quality crystal structure of *syn*-**5**, crystallising in the space group $P6_3/m$, established the stereochemistry and C_{3h} point group symmetry of the *syn* diastereomer.

Anion binding by cavitands (±)-2a–f^{3+}

The anion binding properties of cavitands (±)-**2a**,**d**,**e**$^{3+}$, as revealed by ^{1}H NMR spectroscopic properties of (±)-**2d**$^{3+}$ and the X-ray single crystal structure of (±)-**2d**$[PF_6]_3$·1.5Et_2O·H_2O, were reported in an earlier communication (*9*). These studies will not be repeated here but a summary of the findings is in order.

The solution anion binding properties of cavitands (±)-**2a**,**d**,**e**$^{3+}$ become apparent upon examining the ^{1}H NMR spectra of these hosts. The spectrum of (±)-**2d**$[PF_6]_3$ is particularly diagnostic in that the *para*-substitution pattern of metal-coordinated arene rings provides a good and simple spectroscopic handle to monitor anion complexation in solution. In NO_2Me-d_3 ($\varepsilon = 38$), the *para*-substituted arenes of the upper rim $[(\eta^5\text{-}C_5H_5)Fe^{II}(\eta^6\text{-arene})]^+$ moieties appear as a typical AB pattern, indicative of fast rotation of these groups on the NMR timescale such that the protons on the 'inside' of the cavitand ($H_{\_i}$) are in fast exchange with those on the 'outside' of the cavitand ($H_{\_o}$) (Figure 5). Addition of an excess of halide ions to the solution, in the form of $[NBu_4]Br$, results in the concomitant splitting of the AB pattern into two separate patterns as the rotation of the

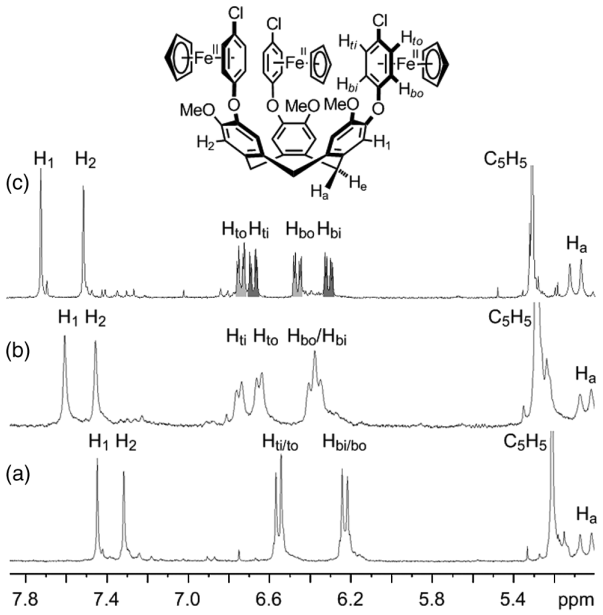

Figure 5. The ^{1}H NMR spectrum of (±)-**2d**$[PF_6]_3$ in (a) NO_2Me-d_3, (b) NO_2Me-d_3 with excess added $[NBu_4]Br$ and (c) acetone-d_6, highlighting the peak splitting that occurs upon anion binding.

$[(\eta^5\text{-}C_5H_5)Fe^{II}(\eta^6\text{-arene})]^+$ moieties is slowed, presumably as a consequence of halide binding within the extended CTB cavity. This behaviour is likely attributed to the formation of a 'penetrated ion pair' (*47*) where the halide ion is bound, reversibly, within the (±)-**2d**$^{3+}$ host cavity. Control experiments show that the addition of excess $[NBu_4][PF_6]$ has little to no effect on the ^{1}H NMR spectrum, suggesting that $[PF_6]^-$ ions are at best weakly bound in NO_2Me-d_3.

In acetone-d_6 ($\varepsilon = 20$), the upper rim $[(\eta^5\text{-}C_5H_5)Fe^{II}(\eta^6\text{-arene})]^+$ moieties of (±)-**2d**$[PF_6]_3$ experience inhibited rotation in the absence of added halide, probably indicating the intracavity binding of a $[PF_6]^-$ anion in this less polar solvent (Figure 5(c)). The actual host–guest binding geometry is likely very similar to that observed in the crystal structure of this salt, which was earlier reported (*9*). The ^{19}F NMR spectrum, however, exhibits only one doublet for the $[PF_6]^-$ anion and therefore bound-to-free anion exchange occurs in the fast exchange domain with respect to the ^{19}F NMR timescale, whereas $[(\eta^5\text{-}C_5H_5)Fe^{II}(\eta^6\text{-arene})]^+$ rotation is slow on the ^{1}H NMR timescale. $[(\eta^5\text{-}C_5H_5)Fe^{II}(\eta^6\text{-arene})]^+$ rotation is therefore not completely coincident with intracavity anion exchange as the ^{1}H and ^{19}F timescales are similar. It is therefore likely that some degree of external $[PF_6]^-$ complexation also occurs in this solvent, contributing to slow rotation of the $[(\eta^5\text{-}C_5H_5)Fe^{II}(\eta^6\text{-arene})]^+$ moieties. This sort of partial ion paring is consistent with a recent study concerning ion pairs of $[(\eta^5\text{-}C_5Me_5)Ru^{II}(\eta^6\text{-arene})][PF_6]$ salts in acetone-d_6 as examined by

$^{19}F-^{1}H$ HOESY and PGSE diffusion NMR experiments (*48*). Halide ($X = Cl^-$, Br^-, I^-) binding by (±)-**2d**$^{3+}$ in acetone-d_6 was previously studied by ^1H NMR titrations and the results suggested that the host has the greatest affinity for iodide (*9*).

The X-ray crystal structures of salts of (±)-**2**$^{3+}$ further demonstrate their ability to complex anions deep within the cavitand bowls. The structure of (±)-**2d**$[PF_6]_3 \cdot 1.5Et_2O \cdot H_2O$ was reported earlier (*9*) and demonstrates a centrally embedded $[PF_6]^-$ ion, with the host adopting a pseudo-C_3 symmetric conformation similar to that observed for the aforementioned (±)-**3a** with all $[(\eta^5\text{-}C_5H_5)Fe^{II}(\eta^6\text{-arene})]^+$ moieties directed 'upward' from the **CTG** bowl. In general, however, cations (±)-**2**$^{3+}$ are difficult to crystallise as their $[PF_6]^-$ or halide salts. Addition of excess $[NBu_4][BF_4]$ to solutions of (±)-**2a–f**$[PF_6]_3$ in acetone, however, results in the precipitation of tetrafluoroborate salts of these hosts. Thus, $[PF_6]^-$ anions can be exchanged for $[BF_4]^-$ using this procedure. Single crystals of the $[BF_4]^-$ salts of (±)-**2d,e** can be obtained when exactly three equivalents of $[NBu_4][BF_4]$ are used. Alternatively, mixed $[PF_6]_x[BF_4]_{3-x}$ salts of (±)-**2**$^{3+}$ can be prepared using $H[BF_4]$ and/or $Na[BF_4]$ in the synthetic work-up and single crystals can be grown by the diffusion of ethers (e.g. THF, Et_2O) into acetone solutions of the mixed salts. By these methods, single crystals of (±)-**2a**$[BF_4][PF_6]_2 \cdot THF \cdot CH_3COCH_3$, (±)-**2d**$[BF_4]_3 \cdot CH_3COCH_3$, (±)-**2e**$[BF_4]_3 \cdot CH_3COCH_3$ and (±)-**2e**$[BF_4]_2[PF_6]_3$ were obtained and their X-ray structures were determined. Summary crystallographic details for these salts are provided in Table 1. Notably, single crystals of salts of (±)-**2b,c**$^{3+}$ could not be obtained, presumably because these compounds are present as a mixture of four diastereomers (*vide supra*).

The crystal structures of (±)-**2d**$[BF_4]_3 \cdot CH_3COCH_3$ and (±)-**2e**$[BF_4]_3 \cdot CH_3COCH_3$ are isostructural, exemplifying the chloro-methyl exchange rule (*49*). Their unit cells and crystal packing are also very similar to those of the mixed salts (±)-**2a**$[BF_4][PF_6]_2 \cdot THF \cdot CH_3COCH_3$ and (±)-**2e**$[BF_4]_2[PF_6]_3$, despite the difference in counterion compositions, upper rim *para*-substituents, and included solvents. The most notable feature in each of these four crystal structures is the presence of a cavity-bound $[BF_4]^-$ anion. The anions rest central to three 'upward' projected $[(\eta^5\text{-}C_5H_5)Fe^{II}(\eta^6\text{-arene})]^+$ moieties of the cavitand (Figure 6) and are deeply buried, with boron positions that lie beneath the mean planes of the iron atoms by, on average, 0.4(1) Å. One comparative measure of the space provided for the anions by the $[(\eta^5\text{-}C_5H_5)Fe^{II}(\eta^6\text{-arene})]^+$ moieties of cavitands (±)-**2a,d–f**$^{3+}$ is the Fe···Fe distance. In (±)-**2d**$[PF_6]_3 \cdot 1.5Et_2O \cdot H_2O$, the $[(\eta^5\text{-}C_5H_5)Fe^{II}(\eta^6\text{-arene})]^+$ moieties adopt positions such that the iron atoms essentially form an isosceles triangle about the guest, with Fe···Fe distances of 8.56, 8.65 and 9.23 Å, defining an area of 33.5 Å^2. These values highlight the slight deviation of the host from ideal C_3 symmetry. In the four structures that exhibit cavity-bound $[BF_4]^-$ anions, the Fe···Fe distances are, on average, slightly shorter, defining triangular areas of 28.2, 30.2, 29.4 and 29.5 Å^2 for (±)-**2a,d–f**$^{3+}$, respectively. The smaller cavity areas, as defined by the iron atoms, reflect the ability of the host to accommodate the smaller anionic guest via a slight contraction.

Coupled with the fact that the $[BF_4]^-$ salts precipitate from acetone, the observation that $[BF_4]^-$ anions are found within the host cavities of the two mixed $[BF_4]^-/[PF_6]$

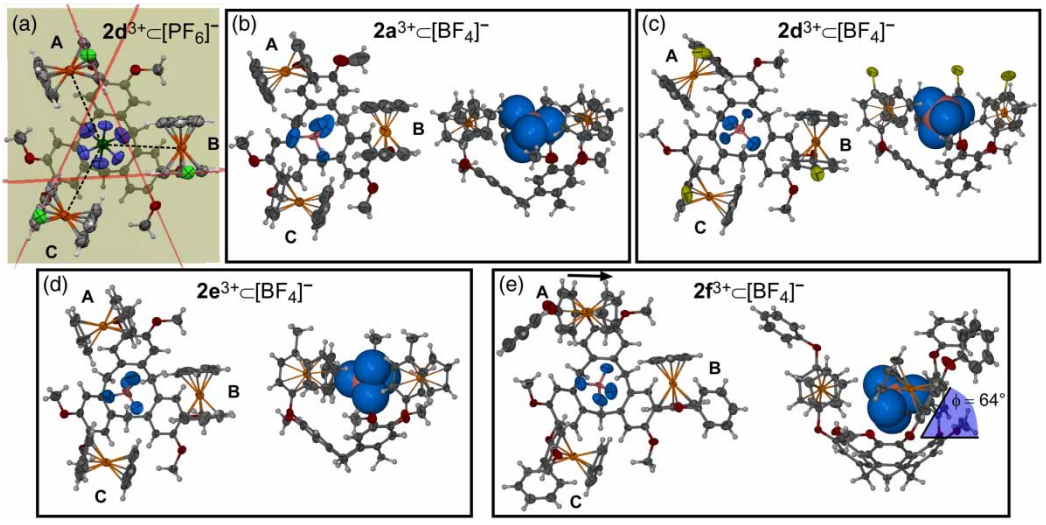

Figure 6. Single crystal X-ray structures of cations (±)-**2**$^{3+}$ and their cavity-bound anions. (a) The [**2d** ⊂ $(PF_6)]^{2+}$ species (*9*), illustrating the planes used to describe the cation conformations; the planes are defined by the arene rings of substituents A, B and C (red), and the oxygen atoms at the upper rim of the cavitand (tan). (b)–(e) 'Top' and 'side' views of the [**2a,d,e,f** ⊂ $(BF_4)]^{2+}$ species, respectively. Only the major occupancy portions of disordered species are shown.

salts seems to suggest a preference of the cavitands (±)-**2a**–**f**$^{2+}$ for this anion. Addition of $[NBu_4][BF_4]$ to acetone-d_6 solutions of (±)-**2d**$[PF_6]_3$ results in only very slight changes in the ^{1}H NMR spectrum before the onset of precipitation. The lack of significant changes in the spectrum ought not necessarily be interpreted as a lack of binding, however, since the environment of the protons *inside* the cavity would be expected to be quite similar in comparing a $[\mathbf{2d} \subset (PF_6^-)]^{2+}$ complex with a $[\mathbf{2d} \subset (BF_4^-)]^{2+}$ complex, as is borne out by the crystallography. It is possible that these hosts do indeed display a greater affinity for the $[BF_4^-]$ ion, which would presumably be attributed to the greater charge density of the smaller anion. Notably, and somewhat surprisingly, the cavity-bound $[BF_4]^-$ anions of these structures all exhibit considerably greater orientational disorder than the corresponding exterior positioned anions in the solid state, even at −100°C. Exactly the opposite effect was observed for the $[PF_6]^-$ salt of (±)-**2d**$^{3+}$, which exhibited a highly ordered, cavity-bound $[PF_6]^-$ anion. Speculation allows one to suppose that a difference in solution binding anion affinity might also be in part attributable to the entropic differences between binding a smaller, orientationally disordered $[BF_4]^-$ anion relative to the larger, more rigidly held $[PF_6]^-$ anion.

It is convenient to designate the three $[(\eta^5\text{-}C_5H_5)Fe^{II}(\eta^6\text{-arene})]^+$ substituents of hosts (±)-**2a,d**–**f**$^{3+}$ with descriptors A–C as shown in Figure 6. In (±)-**2d**$[BF_4]_3\cdot CH_3COCH_3$ and (±)-**2e**$[BF_4]_3\cdot CH_3COCH_3$, the host cation adopts a pseudo-C_3 conformation such that all three $[(\eta^5\text{-}C_5H_5)Fe^{II}]^+$ moieties of the A–C substituents project away from the *ortho*-positioned methoxy substituent, defining an anticlockwise turn with respect to the cavitand enantiomer depicted in Figure 6. In (±)-**2e**$[BF_4]_2[PF_6]_3$, however, one of the three substituents, A (designated with an arrow in Figure 6(e)), is projected 'clockwise' with respect to the cavitand, representing a rotamer of the 'anticlockwise' position. The two substituent conformations differ by essentially a 180° rotation about the $[(\eta^5\text{-}C_5H_5)Fe^{II}(\eta^6\text{-}arene)]^+$—*oxygen* bond and a smaller rotation about the CTB—oxygen bond. The two rotameric conformations reflect the conformational dynamics of the $[(\eta^5\text{-}C_5H_5)Fe^{II}(\eta^6\text{-arene})]^+$ substituents and are not unique to the structure of **2e**$[BF_4]_2[PF_6]_3$. In (±)-**2a**$[BF_4][PF_6]_2\cdot THF\cdot CH_3COCH_3$, two of the substituents (A and C) are disordered such that both rotamers of $[(\eta^5\text{-}C_5H_5)Fe^{II}]^+$ moieties are observed within the crystal (approximately 1:1 and 7:3 anticlockwise:clockwise occupancies, respectively). The disordered situation is not depicted in Figure 6(b); only the anticlockwise positions are shown, which for substituent C is the major occupancy position.

The conformations of the hosts are more quantitatively summarised by measures of the dihedral angles (ϕ) between the mean planes of the arene rings of the A–C substituents (red planes in Figure 6(a)) and the mean planes of the cavitand upper rims, as defined by the oxygen atoms of the diphenyl ether moieties (tan plane in Figure 6(a), Table 2). Of the five available crystal structures of (±)-**2a**,**d**–**f**$^{3+}$ $[BF_4]^-/[PF_6]^-$ salts, including the previously reported (±)-2d$[PF_6]_3\cdot 1.5Et_2O\cdot H_2O$, 14 of the 15 $[(\eta^5\text{-}C_5H_5)Fe^{II}(\eta^6\text{-arene})]^+$ substituents (two disordered) are observed in the 'anticlockwise' conformation. The arenes of the anticlockwise substituents are all nearly normal to the cavitand bowl, with mean ϕ angles of 86(4)°. Each is turned such that the aryl and cyclopentadienyl C—H bonds are directed more-or-less towards the centre of the cavity, allowing the cavity-bound anion to nestle between the planes of the arenes and exposing it to the iron atom. There are four instances (including disordered positions) of substituents in the 'clockwise' rotameric position (see Figure 6(e)). These substituents exhibit mean ϕ angles of 56(9)° reflecting the sterics between the $[(\eta^5\text{-}C_5H_5)Fe^{II}]^+$ moieties and the *ortho*-positioned methoxy substituent in this conformation. In all observed cavitand conformations, the dihedral angles between the phenyl rings of the diphenyl ether moieties are within the normal range for such compounds (*50*).

The five crystal structures of (±)-**2a**,**d**–**f**$^{3+}$ as $[BF_4]^-/[PF_6]^-$ salts allows one to generate statistics with regard to the cation···anion interactions. These interactions are most easily summarised by examining the nonbonded distances between the iron atoms of the $[(\eta^5\text{-}C_5H_5)Fe^{II}(\eta^6\text{-}arene)]^+$ substituents, which bear the greatest positive charge, and the central atom of the spheroidal anions. Table 2 lists the closest three to four Fe···B or Fe···P distances for each of the $[BF_4]^-$ or $[PF_6]^-$ anions found in the five crystal structures of (±)-**2a**,**d**–**f**$^{3+}$. Where disorder of iron or boron atom positions is observed, an average value is listed. The most notable features are as follows. First, the cavity-bound anions are all found to be nestled between the arene rings of the three surrounding $[(\eta^5\text{-}C_5H_5)Fe^{II}(\eta^6\text{-}arene)]^+$ sandwich compounds, being simultaneously exposed to the C—H groups of the arenes and the central iron atoms bearing the bulk of the positive charge. For all structures, the anions within the cavities exhibit the closest set of three Fe···B or Fe···P contacts. For instance, the three closest iron atom distances for the cavity-included $[BF_4]^-$ anions average 4.8(1) Å for the four examples, whereas the three closest iron atom distances of the exterior-positioned $[BF_4]^-$ anions (seven examples) measure 5.6(3) Å. Similarly, the cavity-bound $[PF_6]^-$ anion of (±)-**2d**$[PF_6]_3\cdot 1.5Et_2O\cdot H_2O$, exhibits the closest set of three Fe···P contacts (5.13(4) Å) as compared to the exterior-located $[PF_6]^-$ anions in these structures (5.6(3) Å, five examples). Moreover, in the solid state, only the cavity-bound anions show close contacts to more than one iron atom of the same host molecule. Collectively, these observations strongly support the contention that the central cavity of hosts (±)-**2a**–**f**$^{3+}$

Table 2. Cavitand conformations and closest anion–cation contacts in crystal structures of (±)$\mathbf{2}^{3+}$ salts[a].

(±)-**2a**$[BF_4][PF_6]_2\cdot(THF)\cdot(CH_3COCH_3)$	
$[(C_5H_5)Fe(arene)]^+$conformations[b]	
Substituent	*φ* (°)
A (50%), A′ (50%)	84, 59
B	90
C (70%), C′ (30%)	76, 46
Cavity-bound $[BF_4]^-$	*Distance (Å)*
B1$\cdots$ Fe_A, Fe_B, Fe_C	4.80, 4.76, 4.50
Exterior $[PF_6]^-$	
P1$\cdots$$Fe_A$, Fe_A'', Fe_A''', Fe_B'	5.25, 6.15, 5.85, 5.66
Exterior $[PF_6]^-$	
P2$\cdots$ Fe_B'', Fe_B''', Fe_C, Fe_C'''	6.48, 6.15, 5.41, 5.81
(±)-**2d**$[PF_6]_3\cdot(Et_2O)_{1.5}\cdot H_2O$[c]	
$[(C_5H_5)Fe(arene)]^+$conformations[b]	
Substituent	*φ* (°)
A, B, C	87, 89, 88
Cavity-bound $[PF_6]^-$	*Distance (Å)*
P1$\cdots$ Fe_A, Fe_B Fe_C	5.14, 5.08, 5.16
Exterior $[PF_6]^-$	
P2$\cdots$ Fe_A, Fe_B'', Fe_C'	5.73, 5.88, 5.09
Exterior $[PF_6]^-$	
P3$\cdots$$Fe_A''$, Fe_B', Fe_C	5.12, 5.36, 5.95
(±)-**2d**$[BF_4]_3\cdot(CH_3COCH_3)$	
$[(C_5H_5)Fe(arene)]^+$conformations[b]	
Substituent	*φ* (°)
A, B, C	82, 87, 89
Cavity-bound $[BF_4]^-$	*Distance (Å)*
B1$\cdots$$Fe_A$, Fe_B, Fe_C	4.85, 4.99, 4.88
Exterior $[BF_4]^-$	
B2$\cdots$$Fe_B'''$, Fe_C, Fe_C'	5.93, 5.58, 5.64
Exterior $[BF_4]^-$	
B3$\cdots$ Fe_A', Fe_A'', Fe_A''', Fe_B	5.39, 5.37, 5.47, 4.97
(±)-**2e**$[BF_4]_3\cdot(CH_3COCH_3)$	
$[(C_5H_5)Fe(arene)]^+$conformations[b]	
Substituent	*φ* (°)
A, B, C	88, 89, 84
Cavity-bound $[BF_4]^-$	*Distance (Å)*
B1$\cdots$ Fe_A, Fe_B, Fe_C	4.88, 4.83, 4.89
Exterior $[BF_4]^-$	
B2$\cdots$ Fe_B', Fe_B''', Fe_C, Fe_C''	6.08, 6.45, 5.70, 5.63
Exterior $[BF_4]^-$	
B3$\cdots$$Fe_A$, Fe_A', Fe_A'', Fe_B	5.50, 5.37, 5.50, 5.08
(±)-**2f**$[BF_4]_2[PF_6]$	
$[(C_5H_5)Fe(arene)]^+$conformations[b]	
Substituent	*φ* (°)
A, B, C	64.0, 89, 80
Cavity-bound $[BF_4]^-$	*Distance (Å)*
B1$\cdots$$Fe_A$, Fe_B, Fe_C	4.70, 4.95, 5.05
Exterior $[BF_4]^-$	
B2$\cdots$ Fe_B'', Fe_B''', Fe_C, Fe_C'	5.92, 5.69, 6.51, 5.59
Exterior $[PF_6]^-$	
P1$\cdots$ Fe_A', Fe_B, Fe_C''	5.82, 5.21, 5.74

[a] Each prime (′) mark indicates an interaction distance involving a different cavitand.

is essentially the only significant supramolecular binding site for anions. That is, in the observed host conformations, there are no sites, other than the cavitand cavity, where an anion forms a contact ion pair with more than one [(η^5-C_5H_5)Fe^{II}(η^6-*arene*)]$^+$ moiety of the host.

Host–guest chemistry of cryptophane (±)-anti-5

Cryptophanes commonly form kinetically stable complexes (millisecond or longer lifetimes) with both small neutral molecules and small organic cations in lipophilic solvents (*22*). Thus, a variety of spectroscopic studies were performed to determine whether the new cryptophanes *syn*-**5** or (±)-*anti*-**5** exhibit similar binding properties. In order to reduce competition from the solvent, the studies were performed in deuterated 1,1,2,2-tetrachloroethane (TCE), which was deemed to be too large to be effectively complexed by the host cavity. The crystal structure of (±)-*anti*-**5**, obtained from this solvent, supports this contention as the host does not encapsulate the TCE (*vide infra*). Addition of potential small molecule guests such as CH_2Cl_2, $CHCl_3$, C_6H_6, C_6H_5CN, $NO_2C_6H_6$ results in no changes to the room temperature spectrum of (±)-*anti*-**5**, suggesting that these guests are either not bound, or that they exchange between the solvent and host cavity rapidly on the NMR timescale. Notably, however, each of these molecules (except CH_2Cl_2) forms a solid-state inclusion compound with (±)-*anti*-**5** where the guests are contained within the host cavity (*vide infra*).

Typically, in lipophilic solvents, cryptophane complexes of small cations are more thermodynamically stable than complexes of neutral guests. Other arene-bridged cryptophanes, e.g. those possessing *para*- or *ortho*-xylyl bridges, are known to form kinetically stable complexes with small alkyl ammonium cations at low temperatures (*51*). Specifically, the *anti* diastereomer of the six-carbon, *p*-xylyl-bridged cryptophane (Scheme 1, $R_1 = R_2 =$ OCH_3), forms a more stable [$\Delta G°(210\,K) = -2.9$ kcal/mol] complex with NEt_3Me^+ than with smaller or larger cations. The related four-carbon, *o*-xylyl-bridged cryptophane forms a mildly stable complex with NMe_4^+($\Delta G°$ (210 K) = −0.98 kcal/mol). Under identical conditions (210 K, 9:1 CD_2Cl_2:CD_3OD), however, (±)-*anti*-**5** shows no evidence for complex formation with either $[NMe_4]^+$ or $[NHMe_3]^+$ as their picrate salts.

Snapshots of molecular gating

The inability to observe host–guest complexes of (±)-*anti*-**5** in solution does not imply that the host cavity of this new cryptophane is not capable of encapsulating guests. In fact, a number of crystal structures of (±)-*anti*-**5**, obtained from various solvents of crystallisation, have been determined which shed light on its host–guest chemistry. X-ray crystal structure data for five of these solvates are

given in Table 1. In addition to providing a definitive assignment to ^{1}H NMR spectra of diastereomers *syn*-**5** and (±)-*anti*-**5**, these structures provide general experimental insights into the conformational properties and molecular gating mechanisms of this and other cryptophane container molecules.

The constrictive binding of guests by Cram's hemicarcerand container molecules – i.e. the large $\Delta G^{\ddagger}$ associated with the guest complexation process – has been shown to be attributable to the energy costs associated with the conformational fluctuations necessary to increase the portal size sufficiently for possible guest entrance/escape (*52*). Obviously, analogous, albeit energetically less restricted, processes must occur in the gating of guest molecules by the cryptophane class of container molecules. For cryptophane hosts, two distinct types of conformational processes can be envisaged which would dramatically affect the size and shape of the portals regulating access to the molecular cavity. Firstly, out-of-plane distortions of the methoxy (or other) substituents would provide a larger portal diameter and allow easier exchange of the guest. In keeping with Houk's description of the gating mechanisms of hemicarcerands (*52*), such a process could be described as a 'french door' gate whereby the methoxy groups open outward to allow access to the cavity. The barrier to rotation of the methoxy group in anisole has been the subject of debate, but the coplanar conformation is undoubtedly the minimum energy configuration, implying that there exists a reasonable barrier (a few kcal/mol) to the out-of-plane distortion of each methoxy substituent (*53*). Similarly, other conformational motions of the cryptophanes, such as contortions of the orthocyclophane moieties, conformational adjustments of the bridges or twisting of the two CTB caps about the C_3 axis, might be considered to be analogous to Houk's 'sliding door' gating mechanism described for hemicarcerands. McCammon and co-workers (*54*) have studied the structural fluctuations of a water-soluble hexa acid derivative (*anti*; $R_1 = R_2 = OCH_2COOH$; bridge = $O(CH_2)_3O$) of cryptophane-E by molecular dynamics simulations. The results have been interpreted in terms of a probability controlled, i.e. stochastic, gating process whereby fluctuations of the molecular portals dramatically influence the kinetics of guest binding.

'Open gate' structures

Crystallisation of (±)-*anti*-**5** by diffusion of hexane into a chloroform solution of the host yields a racemic tetrachloroform solvate (±)-*anti*-**5**·$(CHCl_3)_4$. The X-ray crystal structure establishes the *anti* diastereomeric configuration of the host, but, more importantly, shows that one of the chloroform molecules of crystallisation is found encaged within the cryptophane cavity. The (±)-*anti*-**5** ⊂ $CHCl_3$ complex is shown in Figure 7(a). The host conformation can be summarised by a number of simple geometric parameters (Figure 7(f)). One is the 'twist angle', θ, representing the relative turn of the northern and southern CTB caps. Host–guest complexes with different twist angles are reminiscent of the (hemi)carcerplex 'twistomers' observed by Chapman and Sherman (*55*). The twist angle is formally defined by the average dihedral angles subtended by the oxygen atoms of the three bridges with respect to the C_3 (or pseudo-C_3) axis of the host. A zero twist angle therefore represents a conformation wherein the arene bridges lie perfectly normal to both CTB caps, maximising the length (or height) of the cryptophane cavity, *h*. The approximate cavity height can be conveniently measured by the distance between the centres of the arene rings of the two CTB caps. (±)-*Anti*-**5** ⊂ $CHCl_3$ exhibits a minimal (5°) twist angle and the height of the cavity (8.4 Å) is nearly maximised in order to accommodate the encapsulated guest. Notably, unlike the $CHCl_3$ complex of cryptophane-E (Scheme 1, *anti*, $R_1 = R_2 = OCH_3$, bridge = —$O(CH_2)_3O$—), the guest chloroform molecule does not align its C—H bond with the C_3 axis of the host, presumably because of the longer and bulkier bridges of (±)-*anti*-**5**, which cause the long axis of the chloroform molecules to align with the long axis of the host such that two of its chlorine atoms are directed into the two CTB caps.

A closer examination of the host conformation in (±)-*anti*-**5** ⊂ $CHCl_3$ reveals some other remarkable features. Of the six methoxy moieties which help define the portals of the host cavity, four are situated either coplanar with the arene rings to which they are attached or are directed slightly inward such that the diameters of two of the three host portals are minimised. As highlighted in Figure 7(a), however, the two methoxy substituents associated with one of the portals are directed out of the plane of the arene (by 11° and 30°) so as to significantly enlarge the portal diameter. A useful parameter for establishing the size of a portal is the distance between the two methoxy carbon atoms that define it. These distances measure 4.7 and 5.2 Å for the closed portals and 7.8 Å for the 'open' portal in this structure, indicated by the dashed line. Inspection of this portal region reveals the presence of another chloroform molecule essentially perched on the doorstep of the partially opened molecular gate. Thus, it seems that one chloroform molecule is not large enough to effectively fill the cavity volume and allow for efficient packing in the crystal. The host, therefore, gets caught in a 'french door' type of gating conformation with the methoxy groups of one portal stuck slightly open to allow another chloroform to fill the excess volume. Interestingly, the second chloroform molecule directs its C—H towards the face of the bridging arene ring and is seemingly involved in a C—H···π interaction [C(H)···(centroid) = 3.50 Å]. This type of interaction has been of significant interest in supramolecular chemistry and has been calculated to be energetically favourable by ~3 kcal/mol with a C(H)···(centroid) distance of 3.3 Å (*56*).

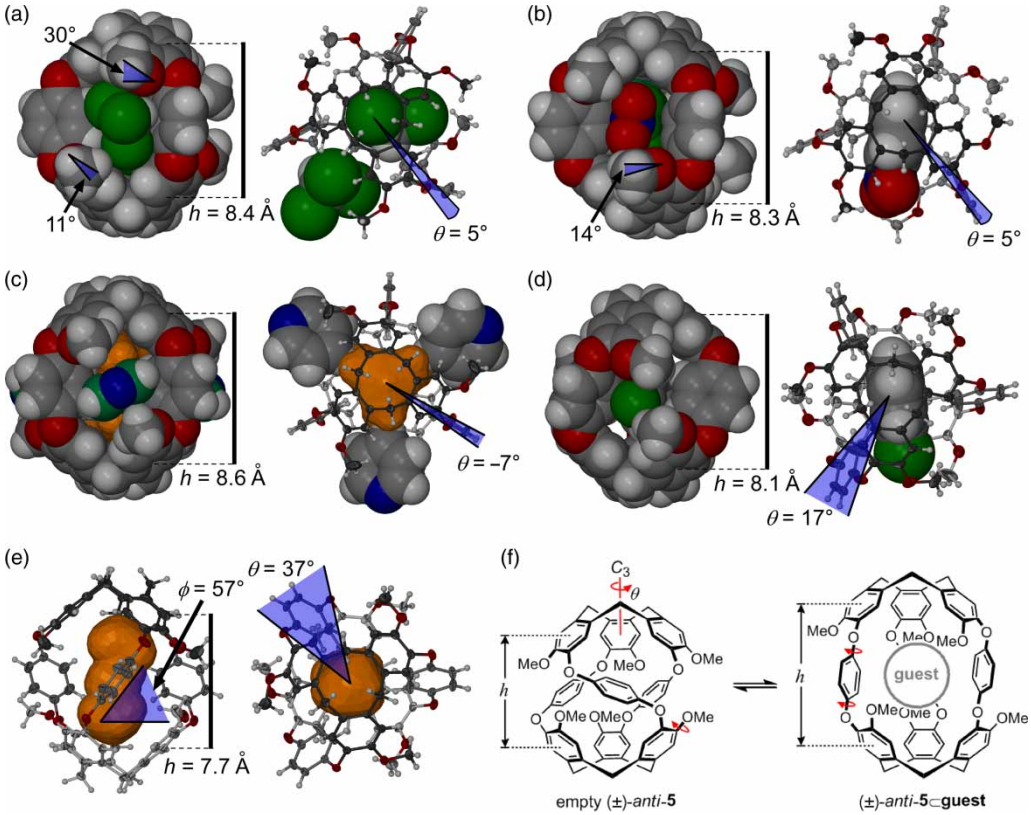

Figure 7. Spacefill and thermal ellipsoid representations of the solvent-encapsulated complexes (a) (±)-*anti*-**5** ⊂ $CHCl_3$·$CHCl_3$, with a molecule of $CHCl_3$ perched at the cavity portal, (b) (±)-*anti*-**5** ⊂ NO_2Ph, (c) (±)-*anti*-**5** ⊂ C_5H_5N·$3C_5H_5N$ (the guest-occupied 116 $Å^3$ central cavity is depicted in orange) and (d) (±)-*anti*-**5** ⊂ C_6H_5Cl, as determined from the crystal structures of the respective solvates. (e) The empty form of (±)-*anti*-**5** from the crystal structure of (±)-*anti*-**5**·$(CHCl_3)_2$·$(TCE)_2$. The empty 52 $Å^3$ cavity is depicted in orange. Principal structural features are highlighted. (f) A summary of the conformational dynamics of (±)-*anti*-**5**.

A similar open 'french door' situation is observed when the host is crystallised with a guest that is just slightly too large for the host cavity. The crystal structure of (±)-*anti*-**5**·$(NO_2C_6H_5)_5$ displays a host conformation similar to that observed in the tetrachloroform solvate with the same twist angle of approximately $\theta = 5°$ (Figure 7(b)). In this structure, however, the host adopts crystallographically imposed C_2 symmetry. One cavity-bound molecule of nitrobenzene is situated centrally within the host cavity with its plane approximately parallel to the cryptophane's pseudo-C_3 axis. The extra bulk of the nitro group precludes its complete encapsulation, however, as this portion of the guest is directed out from the core of the cavity, again through a partially open 'french door' type gate. The two methoxy moieties that define the portal are distorted out of the plane of the arene ring by 14° and the distance between these two carbon atoms is 7.2 Å. The other four methoxy substituents are roughly coplanar with the arene to which they are attached and the C···C distances of these portals are both only 5.3 Å.

From the crystal structure of (±)-*anti*-**5**·$(NO_2C_6H_5)_5$, one might expect that a slightly smaller guest would allow the host to adopt a 'closed gate' type conformation in which all of the methoxy groups lie in the plane of the arene to which they are attached. Thus, (±)-*anti*-**5** was crystallised by ether-induced precipitation from benzene and pyridine to form the isostructural pyridine and benzene solvates. Full details of the pyridine solvate are reported here. The crystals pack in a trigonal crystal system (space group *R*-3*c*) and the high symmetry of the structure exacerbates an extreme disorder of the included solvents. The (±)-*anti*-**5** molecule, however, is well ordered and conforms to ideal, crystallographically imposed D_3 symmetry. Despite the small volume of pyridine, the host adopts its fully extended conformation, displaying a twist angle of only −7° (Figure 7(c)) and giving rise to the most elongated possible cavity ($h = 8.6$ Å). Interestingly, in this extended host conformation, the two orthocyclophane caps of (±)-*anti*-**5** are sufficiently separated to allow three pyridine (or benzene) guests to intercalate between the methoxy groups of each portal and partially penetrate the host cavity. Notably, though, all of the methoxy moieties remain coplanar with their respective arenes (±3°) and the 'french doors' must be considered closed. The portals must nonetheless be considered to be 'open' to the pyridines, as they are

wedged in between the methoxy substituents and are clearly partially within the cryptophane cavity. The C···C distances of the portals are 7.25 Å. This structure can therefore be regarded as a snapshot of a purely 'sliding door' type of gating of guests to (±)-*anti*-**5**, where the portal diameter has been increased, large enough to allow passage of a guest, strictly through twisting of the northern and southern caps.

The portal-situated pyridine positions of (±)-*anti*-**5**·$(C_5H_5N)_{5^2/3}$ are the only solvent locations that could be identified with any degree of crystallographic/chemical certainty. Interstitial sites in the crystal are occupied by what appear to be extremely disordered pyridine molecules and the cryptophane central cavity is occupied by extremely disordered, ill-defined species. SQUEEZE (*57*) estimates an internal cavity bound by the cryptophane and the three portal-situated pyridines of 116 Å^3 with an associated electron count of 21 electrons, a value corresponding exactly to either one half of a pyridine (or diethyl ether). Therefore, either only 50% of the cryptophane cavities are occupied by a solvent molecule or there exists a different species within the cavity, for example, two water molecules (20 electrons). In any case, the ascribed material composition of (±)-*anti*-**5**·$(C_5H_5N)_{5^2/3}$ is not likely to be formally correct, but, in the absence of more information, is sufficient to give a reasonable approximation for the density of the material.

A 'closed gate' structure

Presumably, an optimally sized guest would allow the cryptophane to encapsulate a guest so as to adopt a minimum energy conformation where all of the methoxy substituents lie in the plane of their respective arene rings while the portals remain closed. Such a situation is realised in many of the known crystal structures of cryptophanes, and it was worthwhile to establish whether (±)-*anti*-**5** is capable of doing the same. Co-crystallisation of (±)-*anti*-**5** with a guest intermediate in size between NO_2Ph and benzene (i.e. chlorobenzene) leads to a structure exhibiting a 'closed gate' host conformation, namely (±)-*anti*-**5**·$(C_6H_5Cl)_{2.5}$. Like the other structures of (±)-*anti*-**5**, the guest is located within the host cavity, but the cryptophane host is significantly more twisted ($\theta = 17°$) and the more appropriately sized guest is found to be completely encapsulated by the host (Figure 7(d)). The closed portals are exemplified by the spacefill representation of this complex, which makes it difficult to see the encapsulated guest, and the close C···C separations between the methoxy groups across the portal (4.2, 4.3 and 4.6 Å).

An empty cryptophane container

Single crystals of solvated forms of (±)-*anti*-**5** can also be obtained by the slow diffusion of hexane into solutions of the host in 1,1,2,2-TCE, bromoform, hexachloroacetone or 1:1 TCE:$CHCl_3$. Hexachloroacetone and bromoform were chosen because they were deemed to be too large to possibly reside within the cryptophane cavity. Indeed, in each of these solvates, the cryptophane crystallises with an empty 'cavity', the cryptophane conformation being essentially identical in structure. Only the highest quality of these structure determinations, that of (±)-*anti*-**5**·$(CHCl_3)_2$·$(TCE)_2$, is reported here. It is a curiosity that the 1:1 mixture of $CHCl_3$ and TCE gives rise to crystals of an 'empty' cryptophane, when the former of these guests can clearly fit within the cavity of the host (Figure 7(a)). The crystallographic observation of an empty cryptophane cavity is unprecedented. This behaviour is in stark contrast to the three-carbon-bridged cryptophane-E, which will efficiently scavenge $CHCl_3$ molecules from a solution of TCE. This observation points to a low energetic penalty for the cryptophane being empty vs. occupied, possibly explaining why stable host–guest complexes of (±)-*anti*-**5** are not observed in solution. We (*3*) and others (*2b*,*c*) have found that other cryptophane container molecules tend to conformationally 'implode' in response to the emptying of their cavities. In short, the low energetic penalty for finding (±)-*anti*-**5** to be empty is likely a consequence of the molecules' ability to adopt a conformation that effectively fills most of its own cavity. Indeed, in the crystal structure of (±)-*anti*-**5**·$(CHCl_3)_2$·$(TCE)_2$ (and the other solvates mentioned above), the cryptophane adopts a fully twisted conformation ($\theta = 37°$) in order to minimise the end-to-end length and volume of its internal cavity ($h = 7.7$ Å, Figure 7(e)). The 1,4-diphenoxy bridges are turned inward so as to most effectively fill the void. The symmetry-unique dihedral angles of the bridging arene planes relative to the upper rim of the cavitand measure $\phi = 55°$, 57° and 61°. Each of the methoxy groups lies roughly coplanar to its respective arene and the C···C separations that define the portal size have been reduced to 3.98–4.08 Å. SQUEEZE was used to examine the structure of (±)-*anti*-**5**·$(CHCl_3)_2$·$(TCE)_2$ in order to determine the volume of empty space within the (±)-*anti*-**5** cavity, and to establish that it is in fact devoid of any guest, including the possibility of highly disordered, ill-defined species. SQUEEZE finds discrete, solvent-accessible voids centred within the cryptophane cavities measuring 52 Å^3 and finds no electron density (only two electrons) that can be attributed to any putative species that might be inside. To be sure, the cavities of (±)-*anti*-**5** in crystals of (±)-*anti*-**5**·$(CHCl_3)_2$·$(TCE)_2$ are in fact empty. It is quite rare to observe such large volumes of contiguous empty space in crystalline organic solids owing to their propensity to close pack, and include solvents of crystallisation where necessary in order to fill interstitial voids (*58*).

Conclusions

In summary, aryl-extended **CTG**s (±)-**3a**–**d**,**f** were synthesised from their respective $[(\eta^5\text{-}C_5H_5)Fe^{II}(\eta^6\text{-arene})]^+$-functionalised derivatives (±)-$\mathbf{2}^{3+}$, some of which had been reported previously (*9*). New crystal structures of $[BF_4]^-$ or mixed $[BF_4]^-/[PF_6]^-$ salts of (±)-$\mathbf{2a}$,$\mathbf{d}$–$\mathbf{f}^{3+}$ shed light on the conformations and anion binding properties of these deep cavity cavitands. In general, these molecules adopt a conformation that projects all of the $[(\eta^5\text{-}C_5H_5)Fe^{II}(\eta^6\text{-arene})]^+$ substituents 'up' from the upper rim of the cavitand, creating a deep cavity that is occupied by a $[BF_4]^-$ anion. The host cavities of $\mathbf{2}^{3+}$ appear to show some selectivity for the inclusion of $[BF_4]^-$ in preference to available $[PF_6]^-$ counterions. The crystal structure of (±)-**3a** was also obtained and reveals that, in the solid state, the molecule forms a self-included dimer wherein the cavitand conformation is similar to the conformations observed in structures of $\mathbf{2a}$,$\mathbf{d}$–$\mathbf{f}^{3+}$.

Cryptophanes *syn*-**5** and (±)-*anti*-**5** were synthesised by the photochemically induced demetalation of the putative-metalated cryptophanes *syn*-**4**$[PF_6]_3$ and (±)-*anti*-**4**$[PF_6]_3$, obtained by the synthetic 'capping' of (±)-$\mathbf{2d}^{3+}$ by another molecule of (±)-**CTG**. Single crystal structures of five different solvates of (±)-*anti*-**5** reveal host–guest encapsulated complexes displaying host conformations that can be fairly interpreted as being snapshots of the host involved in the process of molecular gating. The structures provide valuable insights into the guest-gating conformational processes of cryptophane container molecules and can be described in the context of Houk's 'french/sliding' door mechanisms (*52*), originally delineated for hemicarcerand containers. The first crystallographically characterised example of an empty, that is, non-imploded (*3*) cryptophane, that of (±)-*anti*-**5**, reveals that this host can also readily adopt a conformation that fills the bulk of its own cavity, perhaps explaining why this host does not appear to form kinetically stable host–guest encapsulated complexes in solution.

Experimental

Materials and methods

NMR spectra were recorded on a Bruker ARX-250 spectrometer operating at 250.1 MHz (^{1}H), 235.3 MHz (^{19}F), or a Varian Inova 400 MHz spectrometer operating at 400 MHz (^{1}H) or 100.5 MHz (^{13}C). All NMR spectra were collected at room temperature unless otherwise noted and signals were indirectly referenced to tetramethylsilane using residual solvent signals as internal standards. All $[(\eta^5\text{-}C_5H_5)Fe^{II}(\eta^6\text{-arene})][PF_6]$ salts gave expected ^{19}F NMR resonances as a doublet at or near δ −70.68 (d, $^1J_{P\text{-}F} = 708$ Hz, $[PF_6]^-$). Melting points were determined by differential scanning calorimetry using a TA Instruments Q20 operating under a purge of nitrogen at a heating rate of 10°C/min. The melting range is given as the full width at half maximum of peak corresponding to the melting endotherm. Microanalyses were performed by M-H-W Laboratories (Phoenix, AZ, USA).

The $[(\eta^5\text{-}C_5H_5)Fe^{II}(\eta^6\text{-chloroarene})][PF_6]$ starting materials $\mathbf{1a}$–$\mathbf{e}[PF_6]$ were prepared by ligand substitution of ferrocene (Sigma-Aldrich, St. Louis, MO, USA) according to the method of Nesmeyanov (*59*). For all compounds, purification was achieved by passing through a short column of neutral alumina using acetone as an eluent, followed by precipitation with diethyl ether. A typical preparative procedure, that of $\mathbf{1a}[PF_6]$, is given below. Racemic CTG ((±)-**CTG**) was synthesised according to published procedures (*60*). All reactions, unless otherwise stated, were performed under nitrogen atmosphere and in the minimal presence of visible light, but work-up procedures were conducted on the benchtop in the presence of air. All other reagents and solvents were obtained from the usual commercial sources and were used as received. Compounds (±)-$\mathbf{2a}$,$\mathbf{d}$,$\mathbf{e}[PF_6]_3$ were reported previously (*9*), though complete synthetic details are reported herein. Compounds (±)-$\mathbf{2a}$–$\mathbf{h}[PF_6]_3$ are difficult to obtain in high purity and commonly gave disagreeable combustion analyses due to: (i) their photoinstability, (ii) their propensity to include solvents of crystallisation and (iii) the presence of small amounts (<5%) of impurities that are not completely removed during the chromatographic step. Compounds (±)-$\mathbf{2b}$,$\mathbf{c}[PF_6]_3$ were presumed to be obtained as a mixture of the four expected diastereomers, e.g. *RRRM*-$\mathbf{2b}[PF_6]_3$, *RRSM*-$\mathbf{2b}[PF_6]_3$, *RSSM*-$\mathbf{2b}[PF_6]_3$ and *SSSM*-$\mathbf{2b}[PF_6]_3$ and their enantiomers due to the introduction of planar chirality at each of the three 1,2- or 1,3-unsymmetrically substituted $[(\eta^5\text{-}C_5H_5)Fe^{II}(\eta^6\text{-arene})]^+$ moieties (*R*/*S* descriptors in the above notation) and the racemic nature of the helically chiral (±)-**CTG** moieties (*M*/*P* descriptors in the above notation). Consequently, and as expected, (±)-$\mathbf{2b}$,$\mathbf{c}[PF_6]_3$ give rise to complicated and/or broad ^{1}H NMR spectra, as described below. Moreover, the regions of the ^{1}H NMR spectra corresponding to the $[(\eta^5\text{-}C_5H_5)Fe^{II}(\eta^6\text{-arene})]^+$ moieties of (±)-$\mathbf{2a}$–$\mathbf{d}$,$\mathbf{f}[PF_6]_3$ are often further complicated (in, for example, acetone-d_6) by the effects of anion complexation, which serves to freeze out rotation of these groups on the NMR timescale. The near-purity of (±)-$\mathbf{2a}$-$\mathbf{d}$,$\mathbf{f}[PF_6]_3$ is perhaps best evidenced by the typically high yield recovery and complete characterisation of the corresponding photochemically demetalated cavitands (±)-$\mathbf{3a}$–$\mathbf{d}$,$\mathbf{f}$ obtained in pure form.

X-ray crystallography

Single crystal X-ray diffraction data are summarised in Table 1. Crystals were mounted with epoxy on the end of a thin glass fibre, attached to a copper pin and centred in the X-ray beam (Mo Kα) of a Siemens SMART CCD diffractometer equipped with either a 1K or an APEX II

detector and a Siemens LT-2 or an Oxford Cryosystems 700 series variable temperature apparatus regulating the temperature with nitrogen gas. All structures were collected at 173(2) K, with the exception of (±)-*anti*-**5**·5NO_2Ph, which was collected at 100(2) K. Full hemisphere data were collected and accurate unit cells were determined using reflections harvested from the entire data set. Frames were integrated using the program SAINT. Data were corrected for the effects of absorption (SADABS, simulated ψ-scans) and crystal decay where appropriate. All structures were solved (direct methods) and refined using the SHELX suite of software (*61*). Refinement was proceeded using conventional alternating cycles of least-squares refinement (SHELXL-97) on F^2 and difference Fourier synthesis. Whenever possible, all non-hydrogen atoms were refined with anisotropic displacement parameters, while hydrogen atoms were fixed in idealised positions and given displacement parameters in accord to the atom to which they are attached. X-SEED (*62*) was used as a graphical interface to manipulate the model between refinements and to generate figures. Many of the structures exhibited considerable disorder of the anions, including solvents, cyclopentadienyl rings and/or $[(\eta^5\text{-}C_5H_5)Fe(\eta^6\text{-arene})]^+$ moieties. In such instances, efforts were made to implement a refinement model consistent with known molecular geometries by applying reasonable geometric restraints. Occasionally, thermal parameters were also restrained. In general, these refinement restraints lead to higher R-factors, but give rise to more chemically reasonable molecular geometries. In the interest of full disclosure, the instruction files for the final SHELXL refinements are included in the crystallographic information files. (±)-*anti*-**5**·$(C_6H_5N)_{5^{2/3}}$ and (±)-**2a**$[BF_4][PF_6]_2$·(THF)·(CH_3COCH_3) were treated with the SQUEEZE subroutine of Platon (*57*) in order to model highly disordered solvents. The structure of (±)-**2d**$[PF_6]_3$·$(Et_2O)_{1.5}$·(H_2O) has been published previously (*9*). CCDC 782040–782051 contain the supplementary crystallographic data for this paper. These data can be obtained free of charge via ww.ccdc.cam.ac.uk/data_request/cif, by emailing data_request@ccdc.cam.ac.uk or by contacting The Cambridge Crystallographic Data Centre, 12, Union Road, Cambridge CB2 1EZ, UK; Fax: +44-1223-336033.

Syntheses

$[(\eta^5\text{-}C_5H_5)Fe^{II}(\eta^6\text{-}Chloroarene)][PF_6]$ salts

*$[(\eta^5\text{-}C_5H_5)Fe^{II}(\eta^6\text{-}C_6H_5Cl)][PF_6]$, **1a**$[PF_6]$*

To 250 ml of a stirred, room temperature, continuously degassed (N_2) solution of chlorobenzene containing 3.00 g (16.1 mmol) of ferrocene and 0.453 g (16.1 mmol) of aluminium powder was added 8.60 g (64.5 mmol) of $AlCl_3$. A vigorous reaction immediately ensued and the temperature was then raised to near reflux conditions for 3–5 h. The reaction mixture was allowed to cool and was then quenched with *ca.* 100 g of ice (CAUTION!). The bilayered solution was then filtered through Celite and the aqueous layer was separated and repeatedly washed with diethyl ether until the washings were clear. Slow addition of excess $[NH_4][PF_6]$(aq.) to the solution _resulted in the precipitation of **1a**$[PF_6]$ as a yellow solid. The product was removed by filtration, dried under vacuum and passed through a short column of neutral alumina using acetone as an eluent. The pure product (2.43 g, 40%) was precipitated from the acetone by the addition of diethyl ether. The compound gave clean, expected ^1H, ^{13}C and ^{19}F NMR spectra and was not characterised further. Compounds **1b**–**e**$[PF_6]$ were obtained by an identical procedure, though the yields of the other $[(\eta^5\text{-}C_5H_5)Fe^{II}(\eta^6\text{-chloroarene})][PF_6]$ salts are significantly arene dependent.

(±)-2a$[PF_6]_3$

Anhydrous DMF (10 ml) was quickly added to a round bottom flask containing 800 mg (2.11 mmol) of $[CpFe(C_6H_5Cl)][PF_6]$ (**1a**$[PF_6]$), 247 mg (0.605 mmol) of (±)-**CTG** and 584 mg (4.22 mmol) of K_2CO_3 powder. The reaction was stirred overnight at room temperature, under nitrogen and in the absence of visible light, after which it was quenched to slightly acidic pH by the careful addition of 2 M HCl(aq.). To this mixture was slowly added a concentrated aqueous solution of 0.5 equivalents $[NH_4][PF_6]$. At this point, the solution was transparent. Precipitation of the crude product was effected by addition of *ca.* 100 ml of distilled water. This yellow solid was filtered and dried under vacuum (room temperature). The material was further purified by passage through a short column of neutral alumina with acetone, followed by precipitation with diethyl ether. Storage in the absence of light is necessary to avoid decomposition. Yield 711 mg (0.496 mmol), 82%. ^1H NMR (acteone-d_6, *J*/Hz): δ 7.73 (s, 3H), 7.53 (s, 3H), 6.20–6.39 (m, 15H, OC_6H_5), 5.18 (s, 15H, C_5H_5), 5.10 (d, 3H, $^2J = 13.7$ Hz, H_a), 3.93 (d, 3H, $^2J = 13.7$ Hz, H_e), 3.79 (s, 9H, OCH_3). The mixed $[BF_4^-]/[PF_6^-]_2$ salt, for which the crystal structure is reported, was obtained using H$[BF_4]$(aq.) and Na$[BF_4]$ in the place of HCl(aq.) and $[NH_4][PF_6]$ in the above procedure.

(±)-2b$[PF_6]_3$

As for (±)-**2a**$[PF_6]_3$: 1.00 g (2.42 mmol) $[CpFe(o\text{-}C_6H_4Cl_2)][PF_6]$ (**1b**$[PF_6]$), 300 mg (0.734 mmol) (±)-**CTG**, 670 mg (4.85 mmol) K_2CO_3. Yield 858 mg (0.558 mmol), 76%. ^1H NMR (CD_3CN, *J*/Hz): δ 7.49–7.50 (m, 3H), 7.25–7.30 (m, 3H), 6.25–6.65 (m, 3H), 5.95–6.06 (m, 6H), 5.80–5.91 (m, 3H), 4.91–5.15 (m, 15H, C_5H_5 and H_a), 3.87 (d, 3H, $^2J = 14.5$ Hz, H_e),

3.70–3.82 (m, 9H, OCH_3). Note: The spectrum is complicated due to the presence of diastereomers (see text). The spectrum in acetone-d_6 is more complicated.

*(±)-**2c**[PF_6]$_3$*

As for (±)-**2a**[PF_6]$_3$: 2.00 g (4.84 mmol) [CpFe(*m*-$C_6H_4Cl_2$)][PF_6] (**1c**[PF_6]), 565 mg (1.38 mmol) (±)-**CTG**, 1.34 g (9.70 mmol) K_2CO_3. Yield 1.68 g (1.09 mmol), 79%. ^{1}H NMR (CD_3CN, *J*/Hz): ^{1}H NMR (CD_3CN, 250 MHz, *J*/Hz): δ 7.44 (s, 3H, H_1), 7.26 (s, 3H, H_2), 6.43 (d, 3H), 6.35 (d, 3H), 6.23 (t, 3H), 5.99 (t, 3H), 5.09 (s, 15H, C_5H_5), 4.95 (d, 3H, $^2J = 13.9$ Hz, H_a), 3.83 (d, 3H, $^2J = 13.9$ Hz, H_e), 3.76 (s, 9H, OCH_3). Note: The spectrum is complicated due to the presence of diastereomers (see text). The spectrum in acetone-d_6 is more complicated.

*(±)-**2d**[PF_6]$_3$*

As for (±)-**2a**[PF_6]$_3$: 1.00 g (2.42 mmol) [CpFe(*p*-$C_6H_4Cl_2$)][PF_6] (**1d**[PF_6]), 282 mg (0.691 mmol) (±)-**CTG**, 670 mg (4.85 mmol) K_2CO_3. Yield 829 mg (0.539 mmol), 78%. ^{1}H NMR (acetone-d_6, *J*/Hz): δ 7.72 (s, 3H, H_1), 7.52 (s, 3H, H_2), 6.74 (dd, 3H, $^3J = 6.9$ Hz, $^4J = 1.9$ Hz, H_{to}), 6.68 (dd, 3H, $^3J = 6.9$ Hz, $^4J = 1.9$ Hz, H_{ti}), 6.46 (dd, 3H, $^3J = 6.9$ Hz, $^4J = 1.9$ Hz, H_{bo}), 6.31 (dd, 3H, $^3J = 6.9$ Hz, $^4J = 1.9$ Hz, H_{bi}), 5.31 (s, 15H, C_5H_5), 5.10 (d, 3H, $^2J = 13.8$ Hz, H_a), 3.91 (d, 3H, $^2J = 13.8$ Hz, H_e), 3.78 (s, 9H, OCH_3). Note: In acetone-d_6, rotation about the aryl ether bonds is slow relative to the ^{1}H NMR timescale and the protons on the *inside* of the cavitand cavity ($H_{\_i}$) can be distinguished from those on the *outside* of the cavity ($H_{\_o}$) by their response to the addition of halide ions. Aryl protons at the *top* of the cavitand ($H_{t\_}$), adjacent to the 4-chloro substituent, are distinguished from those at the *bottom* of the cavitand ($H_{b\_}$), adjacent to the ethereal oxygen, by 2D COSY experiments.

*(±)-**2e**[PF_6]$_3$*

As for (±)-**2a**[PF_6]$_3$: 200 mg (0.510 mmol) [CpFe(*p*-C_6H_4ClMe)][PF_6] (**1e**[PF_6]), 63 mg (0.154 mmol) (±)-**CTG**, 128 mg (0.926 mmol) K_2CO_3. Yield 170 mg (0.115 mmol), 75%. ^{1}H NMR (acetone-d_6, *J*/Hz): δ 7.71 (s, 3H, H_1), 7.52 (s, 3H, H_2), 6.10–6.31 (m, 12H, $OC_6H_4CH_3$), 5.14 (s, 15H, C_5H_5), 5.09 (d, 3H, $^2J = 13.8$ Hz, H_a), 3.92 (d, 3H, $^2J = 13.8$ Hz, H_e), 3.78 (s, 9H, OCH_3), 2.44 (s, 9H, $OC_6H_4CH_3$).

*(±)-**2f**[PF_6]$_3$*

As for (±)-**2a**[PF_6]$_3$ except that 200 mg (0.130 mmol) of (±)-**2d**[PF_6]$_3$ was used instead of **1a**[PF_6], 55 mg (0.58 mmol) of phenol was used instead of (±)-**CTG**, and 110 mg (0.796 mmol) K_2CO_3 powder was used. Yield 151 mg (0.088 mmol), 68%. ^{1}H NMR (acteone-d_6, *J*/Hz): δ 7.66 (s, 3H, H_1), 7.54 (t, 6H, $^3J = 7.5$ Hz, H_2), 7.50 (s, 3H), 7.35 (t, 3H, $^3J = 7.5$ Hz), 7.28 (d, 6H), 6.22 (~ q, 12H), 5.23 (s, 15H, C_5H_5), 5.06 (d, 3H, $^2J = 13.5$ Hz, H_a), 3.88 (d, 3H, $^2J = 13.5$ Hz, H_e), 3.80 (s, 9H, OCH_3). The mixed [BF_4]$_2$/[PF_6] salt, for which the crystal structure is reported, was obtained using H[BF_4](aq.) and Na[BF_4] in place of HCl(aq.) and [NH_4][PF_6] in the work-up.

2g[PF_6]

As for (±)-**2a**[PF_6]$_3$, except with 600 mg (1.59 mmol) of **1a**[PF_6], 232 mg (1.50 mmol) 4-hydroxy-3-methoxybenzyl alcohol (vanillyl alcohol), 325 mg (2.35 mmol) K_2CO_3 powder. Yield 411 mg (0.828 mmol), 55.2%. ^{1}H NMR (acteone-d_6, *J*/Hz): δ 7.33 (d, 1H, $^3J = 8.1$ Hz, H_f), 7.29 (s, 1H, H_d), 7.09 (d, 1H, $^3J = 8.1$ Hz, H_e), 6.39–6.44 (m, 2H, H_b), 6.25–6.29 (m, 3H, H_a and H_c), 5.21 (s, 5H, C_5H_5), 4.70 (d, 2H, $^3J = 5.1$ Hz, CH_2), 4.31 (t, 1H, $^3J = 5.1$ Hz, O*H*), 3.86 (s, 3H, OCH_3). ^{13}C NMR (acteone-d_6): Aromatic region: δ 151.1; δ 143.0; δ 139.3; δ 133.9; δ 122.3; δ 119.2; δ 111.5; δ 86.7; δ 84.5; δ 77.0; δ 75.7. Aliphatic region: δ 63.0; δ 55.3. ^{1}H NMR peak assignments are according to Figure 3. Single crystals of **2g**[PF_6] were grown by the vapour diffusion of diethyl ether into a dimethylformamide solution of the compound.

2h[PF_6]

As for (±)-**2a**[PF_6]$_3$ except with 250 mg (0.605 mmol) of **1d**[PF_6], 233 mg (1.51 mmol) 4-hydroxy-3-methoxybenzyl alcohol (vanillyl alcohol), 522 mg (3.78 mmol) K_2CO_3 powder. Yield 291 mg (0.0449 mmol), 74.2%. ^{1}H NMR (acteone-d_6, *J*/Hz): δ 7.30 (d, 2H, $^3J = 8.2$ Hz, H_d), 7.28 (s, 2H, H_b), 7.07 (d, 2H, $^3J = 8.2$ Hz, H_c), 6.20 (s, 4H, H_a), 5.24 (s, 5H, C_5H_5), 4.69 (d, 4H, $^3J = 5.6$ Hz, CH_2), 4.33 (t, 2H, $^3J = 5.6$ Hz, O*H*), 3.88 (s, 6H, OCH_3). ^{13}C NMR (acteone-d_6): Aromatic region: δ 151.9; δ 142.9; δ 139.8; δ 131.2; δ 122.2; δ 119.2; δ 111.5; δ 77.8; δ 73.3. Aliphatic region: δ 63.1; δ 55.4. ^{1}H NMR peak assignments are according to Figure 3. Single crystals of **2h**[PF_6]·DMF were grown by the vapour diffusion of diethyl ether into a dimethylformamide solution of the compound.

*(±)-**3a***

In a round bottom flask, 600 mg (0.418 mmol) of (±)-**2a**[PF_6]$_3$ was dissolved in dry, degassed (N_2) acetonitrile (300 ml) and the solution was exposed to direct sunlight. The initially yellow solution turned purple/brown almost immediately, indicating the intermediate formation of [$CpFe(CH_3CN)_3$]$^+$ (*63*), and the reaction was allowed to continue with stirring for 3–4 h. Evaporation of the

solvent, followed by chromatography on silica gel with 1:2 hexane:$CHCl_3$ ($R_f = 0.48$) yielded crude, colourless (±)-**3a**, which was recrystallised by vapour diffusion of hexane into a concentrated toluene solution of the compound. Yield 192 mg (0.301 mmol), 72%. Mp = 216–218°C. ^{1}H NMR (CD_3CN, *J*/Hz): δ 7.29 (t, 6H, $^3J = 7.4$ Hz), 7.14 (s, 3H, H_1), 7.03 (t, 3H, $^3J = 7.4$ Hz), 6.96 (s, 3H, H_2), 6.82 (d, 6H, $^3J = 7.7$ Hz), 4.78 (d, 3H, $^2J = 13.6$ Hz, H_a), 3.64 (s, 9H, OCH_3), 3.60 (d, 3H, $^2J = 13.6$ Hz, H_e). ^{1}H NMR ($CDCl_3$, *J*/Hz): δ 7.28 (d, $^3J = 7.6$ Hz, 6H); δ 7.03 (t, $^3J = 7.6$ Hz, 3H); δ 6.94 (d, $^3J = 8.4$ Hz, 6H); δ 6.90 (s, 3H); δ 6.72 (s, 3H); δ 4.71 (d, $^2J = 13.8$ Hz, 3H, H_a); δ 3.68 (s, 9H, OCH_3); δ 3.51 (d, $^2J = 13.8$ Hz, 3H, H_e). ^{13}C NMR ($CDCl_3$): Aromatic region: δ 157.7; δ 149.7; δ 143.9; δ 135.5; δ 131.8; δ 129.5; δ 122.7; δ 121.4; δ 117.7; δ 114.0. Aliphatic region: δ 56.0; δ 36.3. Anal. calc. for $C_{42}H_{36}O_6$: C, 79.2%; H, 5.70%. Found: C, 78.8%; H, 5.6%. Single crystals of (±)-**3a** were grown by slow evaporation of a toluene solution of the compound.

*(±)-**3b***

As for (±)-**3a**: 800 mg (0.520 mmol) of (±)-**2b**$[PF_6]_3$ yielded 373 mg (0.504 mmol) (±)-**3b**, 97%. Mp = 207–209°C. ^{1}H NMR (acetone-d_6, *J*/Hz): δ 7.48 (dd, 3H, $^3J = 7.9$ Hz, $^4J = 1.6$ Hz), 7.24 (s, 3H, H_1), 7.23 (s, 3H, H_2), 7.19 (td, 3H, $^3J = 7.5$ Hz, $^4J = 1.6$ Hz), 7.05, (td, 3H, $^3J = 7.5$ Hz, $^4J = 1.6$ Hz), 6.74 (dd, 3H, $^3J = 7.5$ Hz, $^4J = 1.6$ Hz), 4.93 (d, 3H, $^2J = 13.5$ Hz, H_a), 3.74 (d, 3H, $^2J = 13.5$ Hz, H_e), 3.69 (s, 9H, OCH_3). ^{13}C NMR (acetone-d_6): Aromatic region: δ 205.5; δ 153.8; δ 149.9; δ 142.7; δ 137.2; δ 132.6; δ 130.3; δ 128.0; δ 123.3; δ 122.2; δ 117.3; δ 114.9. Aliphatic region: δ 55.6; δ 35.4. Anal. calc. for $C_{42}H_{33}O_6Cl_3$: C, 68.2%; H, 4.5%. Found: C, 67.9%; H, 4.7%.

*(±)-**3c***

As for (±)-**3a**: 1.20 g (0.780 mmol) (±)-**2c**$[PF_6]_3$ yielded 560 mg (0.757 mmol) (±)-**3c**, 97%. Mp = 168–171°C. ^{1}H NMR (CD_3CN, *J*/Hz): δ 7.25 (t, 3H, $^3J = 8.1$ Hz), 7.22 (s, 3H, H_1), 7.01–7.06 (dd and s, 6H, H_2 and *para-H*), 6.81 (t, 3H, $^4J = 1.5$ Hz), 6.75 (dd, 3H, $^3J = 8.1$ Hz, $^4J = 1.6$ Hz, H_h), 4.80 (d, 3H, $^2J = 13.6$ Hz, H_a), 3.65 (s, 9H, OCH_3), 3.66 (d, 3H, $^2J = 13.6$ Hz, H_e). ^{1}H NMR ($CDCl_3$): δ 7.17 (t, $^3J = 8.4$ Hz, 3H); δ 6.99 (d, $^3J = 8.4$ Hz, 3H); δ 6.97 (s, 3H); δ 6.91 (s, 3H); δ 6.80 (d, $^3J = 8.4$ Hz, 3H); δ 6.79 (s, 3H); δ 4.75 (d, $^2J = 14.5$ Hz, 3H, H_a); δ 3.69 (s, 9H, OCH_3); δ 3.57 (d, $^2J = 14.5$ Hz, 3H, H_e). ^{13}C NMR ($CDCl_3$): Aromatic region: δ 158.8; δ 150.1; δ 142.8; δ 136.4; δ 134.9; δ 131.9; δ 130.2; δ 122.6; δ 122.4; δ 117.4; δ 115.3; δ 114.3. Aliphatic region: δ 56.1; δ 36.4. Anal. calc. for $C_{42}H_{33}O_6Cl_3$: C, 68.2%; H, 4.5%. Found: C, 68.0%; H, 4.4%.

*(±)-**3d***

As for (±)-**3a**: 380 mg (0.247 mmol) (±)-**2d**$[PF_6]_3$ yielded 176 mg (0.237 mmol) (±)-**3d**, 96%. Mp = 195–198°C. ^{1}H NMR (CD_3CN, *J*/Hz): δ 7.27 (dt, 6H, $^3J = 6.8$ Hz, $^4J = 2.2$ Hz), 7.15 (s, 3H, H_1), 6.99 (s, 3H, H_2), 6.79 (dt, 6H, $^3J = 6.8$ Hz, $^4J = 2.2$ Hz), 4.77 (d, 3H, $^2J = 13.6$ Hz, H_a), 3.65 (s, 9H, OCH_3), 3.60 (d, 3H, $^2J = 13.6$ Hz, H_e). ^{1}H NMR ($CDCl_3$): δ 7.21 (d, $^3J = 8.6$ Hz, 6H); δ 6.91 (s, 3H); δ 6.85 (d, $^3J = 8.6$ Hz, 6H); δ 6.74 (s, 3H); δ 4.72 (d, $^2J = 14.0$ Hz, 3H, H_a); δ 3.69 (s, 9H, OCH_3); δ 3.53 (d, $^2J = 14.0$ Hz, 3H, H_e). ^{13}C NMR ($CDCl_3$): Aromatic region: δ 156.5; δ 149.8; δ 143.5; δ 136.1; δ 131.9; δ 129.4; δ 127.5; δ 121.9; δ 118.6; δ 114.1. Aliphatic region: δ 55.9; δ 36.3. Anal. calc. for $C_{42}H_{33}O_6Cl_{36}$: C, 68.2%; H, 4.5%. Found: C, 68.2%; H, 4.1%.

*(±)-**3f***

As for (±)-**3a**: 89 mg (0.052 mmol) (±)-**2f**$[PF_6]_3$ yielded 33 mg (0.036 mmol) **4.11c**, 69%. Mp = 136–140°C. ^{1}H NMR (acetone-d_6, *J*/Hz): δ 7.33 (dd, 6H, $^3J = 7.6$ Hz, $^3J = 7.6$ Hz); δ 7.23 (s, 3H, H_1); δ 7.17 (s, 3H, H_2); δ 7.06 (t, 3H, $^3J = 7.6$ Hz); δ 6.95 (d, 6H, $^3J = 8.4$ Hz); δ 6.94 (d, 6H, $^3J = 7.6$ Hz); δ 6.87 (d, 6H, $^3J = 8.4$ Hz); δ 4.89 (d, 3H, $^2J = 13.6$ Hz, H_a); δ 3.69 (s, 9H, OCH_3); δ 3.69 (d, 3H, $^2J = 13.6$ Hz, H_e). ^{13}C NMR (acetone-d_6): Aromatic region: δ 158.2; δ 154.4; δ 151.5; δ 150.2; δ 143.6; δ 136.7; δ 132.5; δ 129.7; δ 122.7; δ 122.4; δ 120.4; δ 117.9; δ 117.8; δ 114.8. Aliphatic region: δ 55.5; δ 35.4. Anal. calc. for $C_{60}H_{48}O_9$: C, 78.9%; H, 5.3%. Found: C, 78.7%; H, 5.4%.

*Syn-**5** and (±)-anti-**5***

Two separate solutions of (±)-**CTG** and (±)-**2d**$[PF_6]_3$ (50.0 ml, 6.5 mM, 0.325 mmol each) in DMF were concurrently added via syringe pump over 24 h to a room temperature solution of excess K_2CO_3 in dry, degassed DMF. The mixture was allowed to react for a further 24 h in the dark and was subsequently neutralised with 6 M HCl(aq.), treated with one half of an equivalent of NH_4PF_6(aq.), rotary evaporated (<65°C) to ~35 ml and filtered. Addition of water to the filtrate led to the precipitation of a yellow solid (720 mg) which appeared by ^{1}H NMR spectroscopy to contain mostly polymeric material. The presence of cryptophane products *syn*-**4**$[PF_6]_3$ and (±)-*anti*-**4**$[PF_6]_3$ in this material is demonstrated by the isolation of *syn*-**5** and (±)-*anti*-**5** from its photolysed reaction product (500 ml degassed CH_3CN, sunlight, 5 h; as for (±)-**3a**). Evaporation of the solvent followed by chromatography of the crude, photolysed product on silica gel with $CHCl_3$ yielded crude (±)-*anti*-**5** as a broad, slightly yellow band ($R_f \approx 0.36$). Recrystallisation of this crude material by the partial evaporation of acetone/$CHCl_3$ solution of the compound yielded colour-

less prisms of (±)-*anti*-**5**·*n*solvent, which was heated to 140°C under a nitrogen atmosphere to remove the solvent. Yield 25 mg (7.4%). Mp ≈ 235°C (decomp.). ^{1}H NMR ($CDCl_3$, *J*/Hz) δ 6.94 (s, 6H, H_1), 6.63 (s, 6H, H_2), 6.33 (s, 12H, H_{Ar}), 4.61 (d, 6H, $^2J = 13.8$ Hz, H_a), 3.47 (d, 6H, $^2J = 13.8$ Hz, H_e), 3.39 (s, 18H, H_{OMe}). ^{1}H NMR (DMSO-d_6): δ 7.26 (s, 6H, H_1); δ 7.07 (s, 6H, H_2); δ 6.37 (s, 12H, H_{Ar}); δ 4.71 (d, 6H, $^2J = 13.4$ Hz, H_a); δ 3.55 (d, 6H, $^2J = 13.4$ Hz, H_e) δ 3.35 (s, 18H, OCH_3). ^{13}C NMR (DMSO-d_6): Aromatic region: δ 195.8; δ 151.0; δ 142.4; δ 142.1; δ 135.7; δ 130.3; δ 123.7; δ 116.0. Aliphatic region: δ 56.2; δ 29.1. The material did not give agreeable elemental analyses, presumably related to its high propensity to form thermally unstable solvates of varying composition.

To obtain samples of *syn*-**5**, CH_2Cl_2 was used during the chromatography step, instead of $CHCl_3$, to yield a crude mixture (~2.5:1 by ^{1}H NMR spectroscopy; $R_f \approx 0.64$ for *syn*-**5** and $R_f \approx 0.48$ for (±)-*anti*-**5**) of *syn*-**5** and (±)-*anti*-**5**. These diastereomers could be separated by fractional crystallisation. Diffusion of hexane into $NO_2C_6H_5$ solutions of the crude material yields macroscopic single crystals of (±)-*anti*-**5**·5$NO_2C_6H_5$, for which a single crystal structure was obtained, and microcrystalline *syn*-**5**·*n*$NO_2C_6H_5$ as a fine powder. Repeated recrystallisations yielded *syn*-**5** as a pure $NO_2C_6H_5$ solvate. The nitrobenzene was removed by heating the sample to 140°C under a nitrogen atmosphere. Yield 10 mg (3.0%) of pure material. Mp ≈ 240°C (decomp.). Although not reported here due to the low resolution of the data, an X-ray crystal structure (*syn*-**5**·*n*solvent; hexagonal, $P6_3/m$, $a = 16.8054(13)$Å, $c = 15.5160(16)$Å) was obtained and unequivocally established the identity of the compound as the *syn*-**5** diastereomer. ^{1}H NMR ($CDCl_3$, *J*/Hz): δ 7.02 (s, 6H, H_1), 6.89 (s, 6H, H_2), 6.53 (s, 12H, H_{Ar}), 4.70 (d, 6H, $J^2 = 13.8$ Hz, H_a), 3.50 (d, 6H, $J^2 = 13.8$ Hz, H_e), 3.48 (s, 18H, H_{OMe}). ^{1}H NMR (DMSO-d_6): δ 7.30 (s, 6H, H_1); δ 7.18 (s, 6H, H_2); δ 6.40 (s, 12H, H_{Ar}); δ 4.75 (d, $^2J = 13.4$ Hz, 6H, H_a); δ 3.56 (d, $^2J = 13.4$ Hz, 6H, H_e) δ 3.40 (s, 18H, OCH_3). ^{13}C NMR (DMSO-d_6): Aromatic region: δ 153.5; δ 150.6; δ 142.4; δ 138.1; δ 133.1; δ 124.5; δ 116.1; δ 116.0. Aliphatic region: δ 56.3; δ 35.5. Elemental analysis was not performed due to the paucity of material.

Acknowledgements

This work was supported in part by the US National Science Foundation (DMR-0349316), the University of Missouri and Georgetown University. We thank Prof. Christian Wolf (Georgetown University) for useful advice regarding the notation of stereochemistry for compounds **2b**,**c**$^{3+}$.

References

(1) (a) Grealis, J.P.; Muller-Bunz, H.; Casey M.; McGlinchey, M.J. *Tet. Lett.* **2008**, *9*, 1527–1530. (b) Cannizzaro, S. *Ann. Chem. Pharm.* **1854**, *90*, 252–254. (c) Cannizzaro, S. *Ann. Chem. Pharm.* **1854**, *92*, 113–117.

(2) (a) Even sterically unrestricted CTBs can exist in a nearly isoenergetic, so-called 'saddle-twist' conformation. See, for example: (a) Zimmerman, H.; Tolstoy, P.; Limbach, H.-H.; Puopko, R.; Luz, Z. *J. Phys. Chem. B.* **2004**, *108*, 18772–18778. (b) Garcia, C.; Aubry, A.; Collet, A. *Bull. Soc. Chim. Fr.* **1996**, *133*, 853–867. (c) Huber, G.; Brotin, T.; Dubois, L.; Desvaux, H.; Dutasta, J.-P.; Berthault, P. *J. Am. Chem. Soc.* **2006**, *128*, 6239–6246.

(3) Mough, S.T.; Goeltz, J.C.; Holman, K.T. *Angew. Chem. Int. Ed.* **2004**, *43*, 5631–5635.

(4) Cram, D.J.; Cram, J.M. *Container Molecules and Their Guests*; Ch. 5: Cavitands, Royal Society of Chemistry: Cambridge, 1994.

(5) Hardie, M.J. *Chem. Soc. Rev.* **2010**, *39*, 516–527.

(6) (a) Matsubara, H.; Oguri, S.; Asano, K.; Yamamoto, Y. *Chem. Lett.* **1999**, 431–432. (b) Eckert, J.-F.; Byrne, D.; Nicoud, J.-F.; Oswald, L.; Niergarten, J.-F.; Namuta, M.; Ikeda, A.; Shinkai, S.; Armaroli, N. *New. J. Chem.* **2000**, *24*, 749–758. (c) Hardie, M.J.; Raston, C.L. *Chem. Commun.* **1999**, 1153–1163. (d) Bond, A.M.; Miao, W.; Raston, C.L.; Ness, T.J.; Barnes, M.J.; Atwood, J.L. *J. Phys. Chem. B.* **2001**, *105*, 1687–1695. (e) Huerta, E.; Cequier, E.; de Mendoza, J. *Chem. Commun.* **2007**, 5016. (f) Huerta, E.; Metselaar, G.A.; Fragoso, A.; Santos, E.; Bo, C.; de Mendoza, J. *Angew. Chem. Int. Ed.* **2007**, *46*, 202–205.

(7) Holman, K.T.; Steed, J.W.; Atwood, J.L. *Angew. Chem. Int. Ed.* **1997**, *36*, 1736–1738.

(8) (a) Holman, K.T.; Halihan, M.M.; Steed, J.W.; Jurisson, S.S.; Atwood, J.L. *J. Am. Chem. Soc.* **1995**, *117*, 7848–7849. (b) Holman, K.T.; Halihan, M.M.; Mitchell, A.R.; Burkhalter, R.S.; Steed, J.W; Jurisson, S.S.; Atwood, J.L. *J. Am. Chem. Soc.* **1996**, *118*, 9567–9576.

(9) (a) Holman, K.T.; Orr, G.W.; Steed, J.W.; Atwood, J.L. *Chem. Commun.* **1998**, 2109–2110. (b) Gawenis, J.A.; Holman, K.T.; Atwood, J.L.; Jurisson, S.S. *Inorg. Chem.* **2002**, *41*, 6028–6031.

(10) (a) Steed, J.W.; Holman, K.T.; Atwood, J.L. *Chem. Commun.* **1996**, 1401–1407. (b) Lenthall, J.T.; Steed, J.W. *Coord. Chem. Rev.* **2007**, *251*, 1747–1760.

(11) Fairchild, R.M.; Holman, K.T. *J. Am. Chem. Soc.* **2005**, *127*, 16364–16365.

(12) Collet, A.; Dutasta, J.P.; Lozach, B.; Canceill, J. *Top. Curr. Chem.* **1993**, *165*, 103–129.

(13) Zhang, S.; Palker, A.; Fragoso, A.; Prados, P.; de Mendoza, J.; Echegoyen, L. *Chem. Mater.* **2005**, *17*, 2063–2068.

(14) Gambut, L.; Chauvet, J.-P.; Garcia, C.; Berge, B.; Renault, A.; Riviere, S.; Meunier, J.; Collet, A. *Langmuir.* **1996**, *12*, 5407–5412.

(15) (a) Percec, V.; Imam, M.R.; Peterca, M.; Wilson, D.A.; Heiney, P.A. *J. Am. Chem. Soc.* **2009**, *131*, 1294–1304. (b) Peterca, M.; Percec, V.; Imam, M.R.; Leowanawat, P.; Morimitsu, K.; Heiney, P.A. *J. Am. Chem. Soc.* **2008**, *130*, 14840–14852.

(16) Ider, D.; Heinrich, B.; Guillon, D.; Nicoud, J.-F.; Nierengarten, J.-F. *Chem. Eur. J.* **2000**, *6*, 3501–3507.

(17) (a) Bardelang, D.; Camerel, F.; Ziessel, R.; Schmutz, M.; Hannon, M.J. *J. Mater. Chem.* **2008**, *18*, 489–494. (b) Kubo, Y.; Yoshizumi, W.; Minami, T. *Chem. Lett.* **2008**, *37*, 1238–1239. (c) McKeown, N. B.; Gahnem, B.; Msayib, K.J.; Budd, P.M.; Tattershall, C.E.; Mahmood, K.; Tan, S.; Book, D.; Langmi, W.; Walton, A. *Angew. Chem. Int. Ed.* **2006**, *45*, 1804–1807. (d) Westcott, A.; Sumby, C.J.; Walshaw, R.D.; Hardie, M.J. *New J. Chem.* **2009**, *33*, 902–912.

(18) (a) Structural Aspects of Inclusion Compounds Formed by Organic Host Lattices. In *Inclusion Compounds*; Atwood, J.L., Davies, J.E.D., MacNicol, D.D., Eds.; Academic Press: London, 1984; Vol. 2; pp 91–121. (b) Hardie, M.J.; Nichols, P.J.; Raston, C.L. *Supramol. Chem.* **2002**, *8*, 1–41.
(19) (a) Mough, S.T.; Holman, K.T. *Chem. Commun.* **2008**, 1407–1409. (b) Sumby, C.J.; Fisher, J.; Prior, T.J.; Hardie, M.J. *Chem. Eur. J.* **2006**, *12*, 2945–2959.
(20) (a) Clark, T.E.; Makha, M.; Sobolev, A.N.; Raston, C.L. *J. Chem. Soc., Dalton Trans.* **2008**, *36*, 4855–4859. (b) Hardie, M.J.; Raston, C.L. *Angew. Chem. Int. Ed.* **2000**, *39*, 3835–3839.
(21) (a) McKeown, N.B.; Gahnem, B.; Msayib, K.J.; Budd, P.M.; Tattershall, C.E.; Mahmood, K.; Tan, S.; Book, D.; Langmi, H. W.; Walton, A. *Angew. Chem. Int. Ed.* **2006**, *45*, 1804–1807. (b) Budd, P.M.; Butler, A.; Selbie, J.; Mahmood, K.; McKeown, N.B.; Ghanem, B.; Msayib, K.; Book, D.; Walton, A. *Phys. Chem. Chem. Phys.* **2007**, *9*, 1802–1808.
(22) (a) Holman, K.T. in *Encyclopedia of Supramolecular Chemistry*, Atwood, J.L., Steed J.W., Eds.; Dekker: New York, 2004; Vol. 1; pp 340–348. (b) Collet, A. In *Comprehensive Supramolecular Chemistry*, Atwood, J.L., Davies, J.E.D., MacNicol, D.D., Vogtle, F., Eds.; Permagon: Oxford, 1996; Vol. 2; pp 325–365.
(23) Brotin, T.; Dutasta, J.-P. *Chem. Rev.* **2009**, *109*, 88–130.
(24) Xu, D.; Warmuth, R. *J. Am. Chem. Soc.* **2008**, *130*, 7520–7521.
(25) Zhong, Z.; Ikeda, A.; Shinkai, S.; Sakamoto, S.; Yamaguchi, K. *Org. Lett.* **2001**, *3*, 1085–1087.
(26) (a) Ronson, T.K.; Fisher, J.; Harding, L.P.; Rizkallah, P.J.; Pierre, J.; Warren, J.E.; Hardie, M.K. *Nat. Chem.* **2009**, *1*, 212–216. (b) Ronson, T.K.; Carruthers, C.; Fisher, J.; Brotin, T.; Harding, L.P.; Rizkallah, P.J.; Hardie, M.J. *Inorg. Chem.* **2010**, *49*, 675–685. (c) Abrahams, B.F.; FitzGerald, N.J.; Robson, R. *Angew. Chem. Int. Ed.* **2010**, *49*, 2896–2899.
(27) (a) Jasat, S.; Sherman, J.C. *Chem. Rev.* **1999**, *99*, 931–968. (b) Conn, M.M.; Rebek, J. *Chem. Rev.* **1997**, *97*, 1647–1668.
(28) Collet, A. Cyclotriveratrylene and Related Hosts. In *Comprehensive Supramolecular Chemistry*; Atwood, J.L., Davies, J.E.D., MacNicol, D.D., Vogtle, F., Eds.; Permagon: Oxford, 1996; Vol. 9, pp 281–302.
(29) (a) Sessler, J.L.; Gale, P.A.; Cho, W.-S. *Anion Receptor Chemistry*; Royal Society of Chemistry: Cambridge, 2006. (b) Steed, J.W. Chem. Soc. Rev. **2009**, *38*, 506–519.
(30) Staffilani, M.; Hancock, K.S.B.; Steed, J.W.; Holman, K.T.; Atwood, J.L.; Juneja, R.K.; Burkhalter, R.S. *J. Am. Chem. Soc.* **1997**, *119*, 6324–6335.
(31) Arduini, A.; Calzavacca, F.; Demuru, D.; Pochini, A.; Secchi, A. *J. Org. Chem.* **2004**, *69*, 1386–1388.
(32) (a) Beer, P. D.; Cadman, J. *Coord. Chem. Rev.* **2000**, *205*, 131–155. (b) Beer, P.D.; Hayes, E.J. *Coord. Chem. Rev.* **2003**, *240*, 167–189.
(33) Hay, B.P.; Bryantsev, V.S. *Chem. Commun.* **2008**, 2417–2428.
(34) (a) Reith, S.; Bao, X.; Wang, B.-Y.; Hadad, C.M.; Badjic, J.D. *J. Am. Chem. Soc.* **2010**, *132*, 773–773. (b) Rieth, S.; Wang, B.-Y.; Bao, X.; Badjic, J.D. *Org. Lett.* **2009**, *11*, 2495–2498. (c) Wang, B.-Y.; Rieth, S.; Badjic, J.D. *J. Am. Chem. Soc.* **2009**, *131*, 7250–7252.
(35) Takeuchi, D.; Asano, I.; Osakada, K. *J. Org. Chem.* **2006**, *71*, 8614–8617.
(36) (a) Das, D.; Barbour, L.J. *Chem. Commun.* **2008**, 5110–5112. (b) Das, D.; Barbour, L.J. *J. Am. Chem. Soc.* **2008**, *130*, 14032–14033.
(37) Astruc, D. *Top. Curr. Chem.* **1991**, *160*, 47–95.
(38) Abd-El-Aziz, A.S.; de Denus, C.R.; Zaworotko, M.J.; MacGillivray, L.R. *J. Chem. Soc. Dalton Trans.* **1995**, 3375–3393.
(39) Abd-El-Aziz, A.; de Denus, C.R.; Zaworotko, M.J.; Sharma, C.V.K. *Chem. Commun.* **1998**, 265–266.
(40) (a) Gill, T.P; Mann, K.R. *Inorg. Chem.* **1980**, *19*, 3007–3010. (b) Gill, T.P.; Mann, K.R. *Inorg. Chem.* **1983**, *22*, 1986–1991. (c) McNair, A.M.; Schrenk, J.L.; Mann, K.R. *Inorg. Chem.* **1984**, *23*, 2633–2640. (d) Schrenk, J.L.; McNair, A.; M.; McCormick, F.B.; Mann, K.R. *Inorg. Chem.* **1986**, *25*, 3501–3504.
(41) Chao, J.; Desando, M.A.; Gourlay, D.L.; Orr, D.E.; Walker, S. *J. Phys. Chem.* **1984**, *88*, 711–716.
(42) Steed, J.W.; Zhang, H.M.; Atwood, J.L. *Supramol. Chem.* **1996**, *7*, 37–45.
(43) (a) Frensch, K.; Vögtle, F. *Liebigs Ann. Chem.* **1979**, 2121–2123. (b) Canceill, J.; Collet, A. *Nouv. J. Chem.* **1986**, *10*, 17. (c) Garcia, C.; Andraud, C.; Collet, A. *Supramol. Chem.* **1992**, *1*, 31–45. (d) Garcia, C.; Malthête, J.; Collet, A. *Bull. Soc. Chim. Fr.* **1993**, *130*, 93–95.
(44) Canceill, J.; Collet, A. *J. Chem. Soc., Chem. Commun.* **1988**, 582.
(45) Cram, D.J.; Tanner, M.E.; Keipert, S.J.; Knobler, C.B. *J. Am. Chem. Soc.* **1991**, *113*, 8909–8916.
(46) (a) Fogarty, H.A.; Berthault, P.; Brotin, T.; Huber, G.; Desvaux, H.; Dutasta, J.-P. *J. Am. Chem. Soc.* **2007**, *129*, 10332–10333. (b) Traore, T.; Delacour, L.; Garcia-Argote, S.; Berthault, P.; Cintrat, J.-C.; Rousseau, B. *Org. Lett.* **2010**, *12*, 960–962.
(47) (a) Boche, G. *Angew. Chem. Int. Ed. Engl.* **1992**, *31*, 731–732. (b) Abbott, A.P.; Schiffrin, D.J. *J. Chem. Soc., Faraday Trans.* **1990**, *86*, 1453–1459.
(48) Moreno, A.; Pregosin, P.S.; Veiros, L.F.; Albinati, A.; Rizzato, S. *Chem. Eur. J.* **2008**, *14*, 5617–5629.
(49) Desiraju, G.R.; Sarma, J.A.R.P. *Proc. Indian Acad. Sci. (Chem. Sci.)* **1986**, *96*, 599–605.
(50) Straßner, T. *Can. J. Chem.* **1997**, *75*, 1011–1022.
(51) Miura, M.; Yuzawa, S.; Takeda, M.; Takeda, M.; Habata, Y.; Tanase, T.; Akabori, S. *Supramol. Chem.* **1996**, *8*, 53–66.
(52) (a) Nakamura, K.; Houk. K.J. *Am. Chem. Soc.* **1995**, *117*, 1853–1854. (b) Houk, K.N.; Nakamura, K.; Sheu, C.; Keating, A.E. *Science* **1996**, *273*, 627–629. (c) Rouhi, M. *Chem. Eng. News.* **1996**, *74*, 4. (d) Sheu, C.; Houk, K. *J. Am. Chem. Soc.* **1996**, *118*, 8056–8070.
(53) (a) Vincent, M.A.; Hillier, I.H. *Chem. Phys.* **1990**, *140*, 35–40. (b) Spellmeyer, D.C.; Grootenhuis, P.D.J.; Miller, M.D.; Kuyper, L.F.; Kollman, P.A. *J. Phys. Chem.* **1990**, *94*, 4483–4491. (c) Schaefer, T; Sebastian, R. *Can. J. Chem.* **1989**, *67*, 1148–1152.
(54) (a) Kirchhoff, P.D.; Bass, M.B.; Hanks, B.A.; Collet, A.; McCammon, J.A. *J. Am. Chem. Soc.* **1996**, *118*, 3237–3246. (b) Kirchhoff, P.D.; Dutasta, J.-P.; Collet, A.; McCammon, J.A. *J. Am. Chem. Soc.* **1997**, *119*, 8015–8022.
(55) Chapman, R.G.; Sherman, J.C. *J. Am. Chem. Soc.* **1999**, *121*, 1962–1963.
(56) Jorgensen, W.L.; Severence, D.L. *J. Am. Chem. Soc.* **1990**, *112*, 4768–4774.
(57) (a) Spek, A. *J. Appl. Crystallogr.* **2003**, *36*, 7. (b) Spek, A.L. *Acta Cryst. A.* **1990**, *A46*, C34.

(58) (a) Atwood, J.L.; Barbour, L.J. *Science* **2002**, *296*, 2367–2369. (b) Barbour, L.J. *Chem. Commun.* **2006**, 1163–1168.
(59) (a) Nesmeyanov, A.N.; Vol'kenau, N.A.; Bolesova, I.N. *Tetrahedron Lett.* **1963**, 1725–1729. (b) Nesmeyanov, A.N.; Vol'kenau, N.A.; Bolesova, I.N. *Dokl. Akad. Nauk SSSR* **1963**, *149*, 615. (c) Nesmeyanov, A.N.; Vol'kenau, N.A.; Bolesova, I.N. *Dokl. Akad. Nauk SSSR* **1966**, *166*, 607–611. (d) Nesmeyanov, A.N.; Vol'kenau, N.A.; Shilovtseva, L.S. *Dokl. Akad. Nauk SSSR* **1965**, *160*, 1327–1332.
(60) (a) Canceill, J.; Gabard, J.; Collet, A. *J. Chem. Soc., Chem. Commun.* **1983**, 122–123. (b) Canceill, J.; Collet, A.; Gotarelli, G. *J. Am. Chem. Soc.* **1984**, *106*, 5997–6003.
(61) Sheldrick, G.M. *Acta Cryst. A.* **2008**, *64*, 112–122.
(62) (a) Barbour, L.J. *Supramol. Chem.* **2001**, *1*, 189–191. (b) http://x-seed.net.
(63) Freedman, D.A.; Gill, T.P.; Blough, A.M.; Koefod, R.S.; Mann, K.R. *Inorg. Chem.* **1997**, *36*, 95–102.